CHAPTER 4

OPTICS AND SINGLE PARTICLE DYNAMICS

All optics descriptions in this Chapter refer to the LHC Version 6.4 including the repositioning [1] of the Q3 triplet magnets which is part of Version 6.5. [1]

The LHC optics design follows a modular approach where the functionality of each insertion is extended by one arc-cell on each side of the insertion [2]. This approach allows an optics matching with fixed and equal phase advances over the insertions for both beams that does not perturb the optics in the rest of the machine. The total tune of the machine is adjusted via the arc cell optics. In conjunction with the series powering of the Ring 1 and Ring 2 quadrupole magnets this approach automatically generates the same tunes for both beams. The flexibility of the phase advance over the insertions provides a measure for the flexibility of the total LHC optics and the range over which the phase advance between the main experimental insertions can be changed.

The common low-β triplets in the experimental insertions provide opposite focusing for the two counter-rotating beams. A strictly antisymmetric powering was adopted for the feasibility study as a natural symmetry for a proton-proton machine with common magnetic elements [3]. However, in the present optics design the antisymmetric powering is only approximately kept, except in the low-beta triplets where it is exact.

Table 4.1: Horizontal and vertical phase advances in the LHC for the injection optics. All values given below, except tor the phase advances given for IR3 and IR7, correspond to the LHC V6.4 optics. The values given for IR3 and IR7 correspond to the new cleaning insertion optics that will be part of V6.5. The new IR3 and IR7 optics have different phase advances for Beam 1 and Beam 2. The values for Beam 1 are given on top and the values for Beam 2 on the bottom of the double entries. The difference between the Beam 1 and Beam 2 phase advance needs to be compensated in the other insertions.

	1 arc (21 cells)	IR1/IR5	IR2	IR3	IR4	IR6	IR7	IR8	total insertions	LHC total
$\frac{\triangle\mu_x}{2\pi}$	5.497250	2.618	2.991	2.307 2.285	2.143	2.015	2.382 2.492	3.204	20.302	64.28
$\frac{\triangle\mu_y}{2\pi}$	5.099375	2.644	2.844	1.897 1.932	1.870	1.780	1.968 2.090	2.804	18.515	59.31

4.1 ARC OPTICS

The LHC arc cells feature a FODO lattice with approximately 90° phase advance per cell in both planes. A perfect 90° lattice generates equal tunes in the horizontal and vertical planes (apart from phase advance differences generated in the insertion regions) and minimizes the optics perturbations by tuning the trim quadrupole circuits at the end of each arc [4]. However, a correction of the systematic coupling generated by the main dipole field errors favors an optics with an integer tune split between the horizontal and vertical tunes [5] [6]. An integer tune split of 7 or 8 units is optimal for the compensation of the systematic resonances in each arc [7]-[10].

However, such a large tune split also implies a dephasing of the four sextupole families in each arc and reduces the margins for the magnet strength (in the plane with the higher tune value) and aperture (in the plane with the smaller tune value). Following V6.2 of the LHC lattice the optics is based on a total integer tune split of 5 units which is the combined results of the differences in the horizontal and vertical phase advances in the arcs and the insertion regions. This solution presents a good compromise between operational margins for the magnet strengths, aperture and a compensation efficiency of systematic resonances. Tab 4.1 summarizes the different contributions to the integer tune split and Fig 4.1 the corresponding optic functions of the LHC arc cells. All values given in Tab 4.1, except for the phase advances in IR3 and IR7, correspond to the LHC V6.4

[1] A summary of the differences between different LHC version can be found on the WWW under: http://slap.web.cern.ch/slap/MAC.pdf

optics. The values given for IR3 and IR7 correspond to the new cleaning insertion optics that will be part of V6.5. The new IR3 and IR7 optics have different phase advances for Beam 1 and Beam 2. The difference between the Beam 1 and Beam 2 phase advance needs to be compensated in the other insertions.

Fig 4.2 shows the mechanical acceptance of the arc cell in terms of n_1. The smallest acceptance depends on the spurious dispersion along the machine and Fig 4.2 shows the worst case of the mid-arc cells ($n_1 = 6.75$ for mid-arc cell-12 in Beam 2) for the nominal injection optics (a definition for n_1 can be found in Sec 4.3). This value is slightly smaller than the specification of $n_1 = 7.0$ (see Sec. 4.3 and Chap. 18 for details on the aperture specifications) and might require a revision of the mechanical tolerances for the dipole geometry.

Fig 4.3 and 4.4 show the variation of the horizontal and vertical tunes versus the relative beam momentum deviation for the perfect linear lattice with lattice sextupole magnets and a correction of the chromaticity for the injection and the collision optics with two squeezed IRs (IR1 and IR5), respectively. No magnetic field errors are considered here. One clearly sees how the chromaticity shows a strong third order dependence for the collision optics.

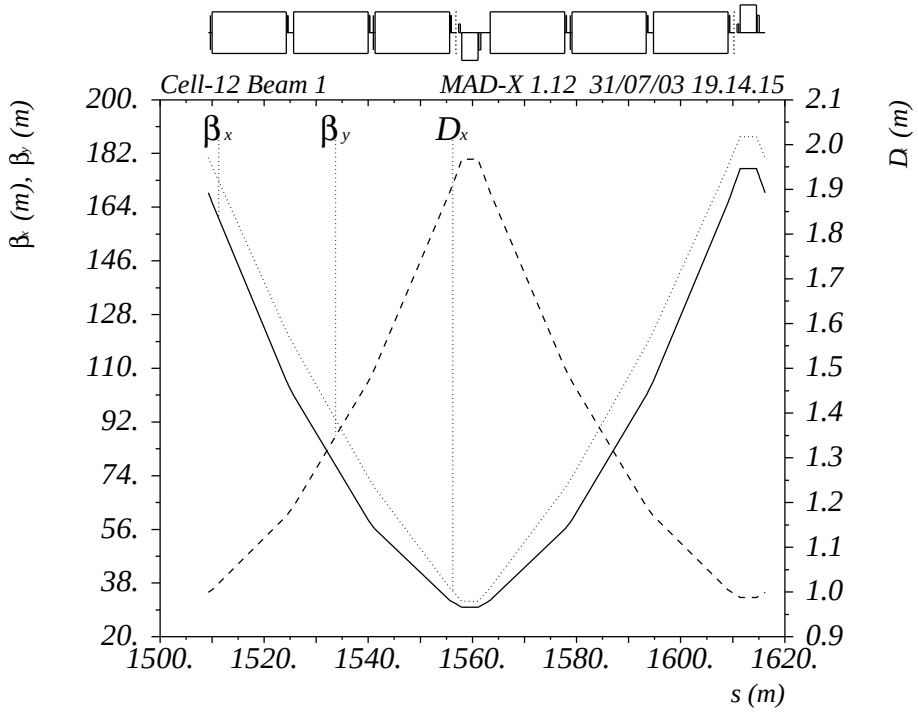

Figure 4.1: Periodic optics solution for the worst case LHC arc cell.

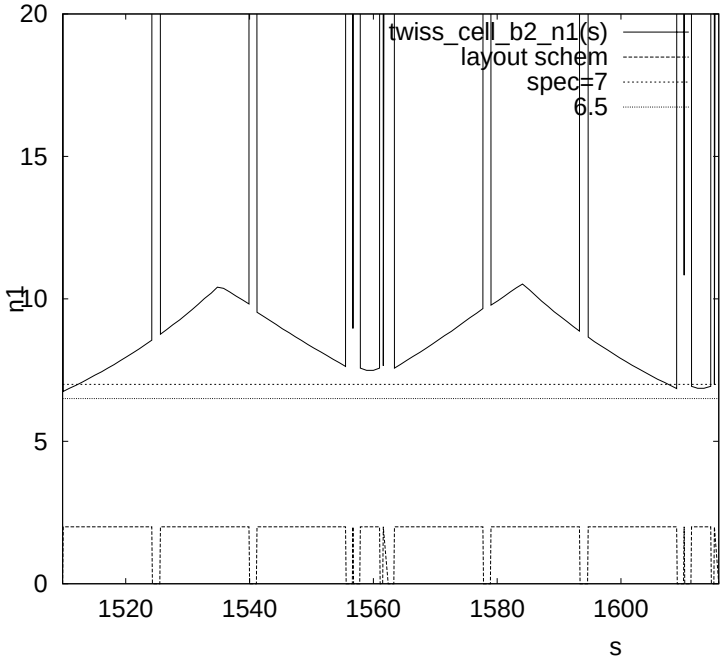

Figure 4.2: Periodic optics solution of a LHC arc cell

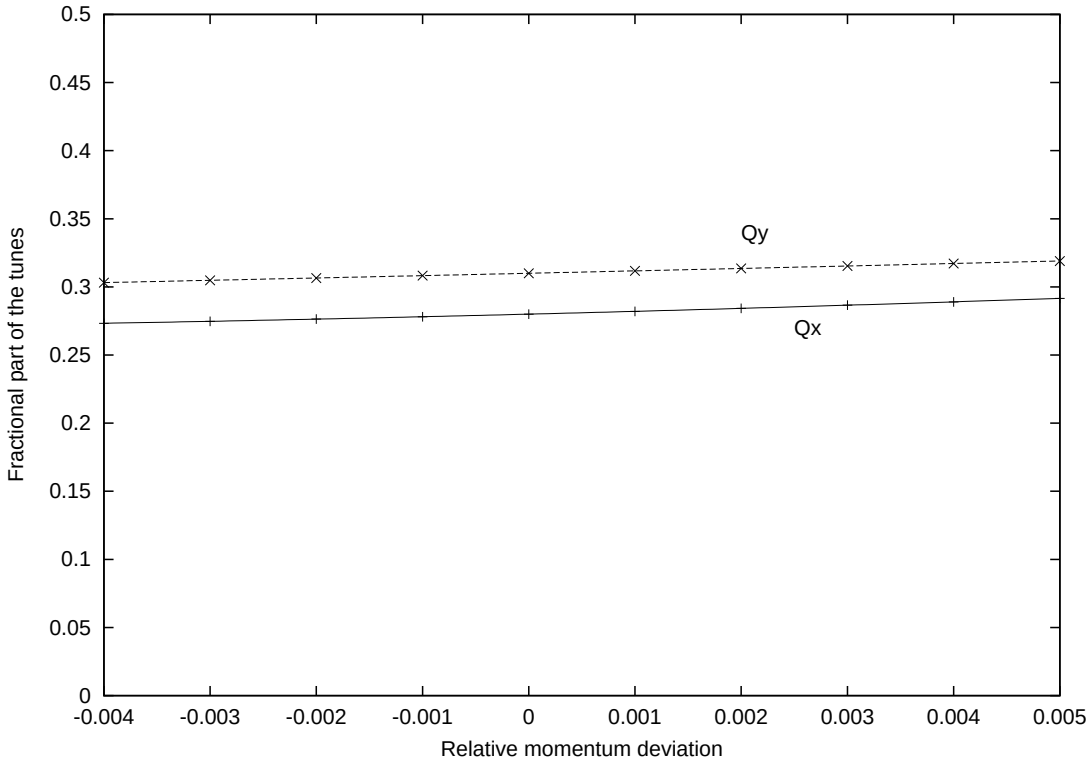

Figure 4.3: Tune variations versus the relative momentum offset for the unperturbed linear lattice with lattice sextupole magnets and corrected chromaticity for the injection optics without multipole errors.

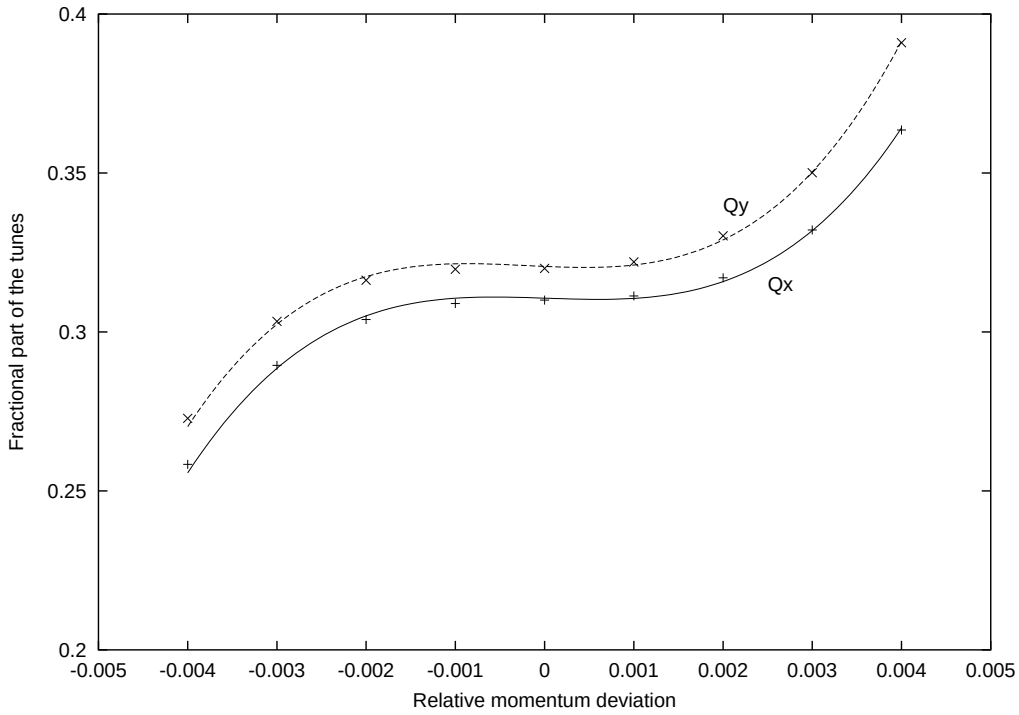

Figure 4.4: Tune variations versus the relative momentum offset for the unperturbed linear lattice with lattice sextupole magnets and corrected chromaticity for the collision optics with IR1 and IR5 squeezed to $\beta^* = 0.55$m without multipole errors.

Table 4.2: Crossing angle and orbit at IP1 for Beam 1 (half the total beam separation). The minimum separation between Beam 1 and Beam 2 is specified for one plane. The state 'Injection' refers to the optics configuration during injection, 'Ramp' to the configuration during ramp, 'Pre-Collision' to the optics at the end of the ramp but before the low-β squeeze and 'Collision' to the optics configuration at top energy after the low-β squeeze.

State	$\beta^*_{x,y}$ (m)	vertical crossing angle (μrad)	horizontal orbit (mm)	$d_{\rm IP}$ (σ)	$d_{\rm min}$ (σ)
Injection	18.0	+ 160.0	- 2.50	13.3	10.5
Ramp	18.0	+ 40.0	- 0.625	13.3	10.5
Pre-collision	0.55	+ 142.5	- 0.50	60	6.9
Collision	0.55	+ 142.5	- 0.0	0.0	6.9

4.2 INSERTION OPTICS

4.2.1 Crossing angle summary

The main limit on the bunch intensity will eventually come from beam-beam effects. To allow a maximum number of bunches, they are closely spaced (25 ns) and in order to avoid unwanted collisions in the part where the two beams share a common vacuum chamber in all experimental interaction regions, the beams must collide at a small crossing angle. Since the common part is much longer than the bunch spacing, parasitic collisions, so-called long-range interactions, of the separated beams cannot be avoided (see Sec. 5.9). With the present geometry, 15 unwanted long-range encounters occur on each side of a collision point, i.e. 120 for all collision points. The crossing angle has to provide a sufficient separation at all parasitic encounters to keep the effects small from long-range beam-beam interactions and should allow a quasi head-on collision at the central interaction point. This is true in particular for the two low β^* interaction regions IR1 and IR5 where the long-range effects are strongest (see Sec. 5.9). The normalized beam separation should not be smaller than 7 σ at any of the parasitic encounters. Before the two beams are brought into collision, i.e. for injection and the energy ramp, the central head-on collision must also be avoided. This is done with a parallel separation bump in the plane orthogonal to the crossing plane. This bump must also serve as a handle to push the beams into collision and to adjust the collision point in this plane, if necessary. To that purpose it is mandatory that the two beams can be steered independently. To compensate part of the unwanted beam-beam effects the crossing angles in the two low-β^* interaction regions IR1 and IR5 should be in orthogonal planes (see Sec. 5.9). At present it is assumed that the beams cross at a vertical angle in IR1 and in the horizontal plane in IR5. The boundary conditions and the strategy for the crossing scheme are summarized in [11].

Additional considerations are required for IR2 and IR8, housing the ALICE and LHCb experiments. The β^* in these interaction regions are much larger and the detrimental effects of long-range interactions are much smaller. However, the layout of the experiments constrain the choice of the beam separation scheme. Both experiments operate spectrometer magnets with magnetic fields orthogonal to the LHC beams. Together with their compensation magnets they form antisymmetric bumps with a crossing angle at the interaction points [12]. Furthermore, the separation schemes must allow a polarity change of both spectrometers. These internal crossing angles are in the vertical (ALICE, $\theta = \pm 70$ μrad) and horizontal plane (LHCb, $\theta = \pm 135$ μrad) but their longitudinal extension is not large enough to separate the beams at all parasitic encounters. Additional separation has to be provided by external crossing angles and parallel bumps similar to those in interaction points 1 and 5. In the present design these crossing angles are in the same plane as the angles from the spectrometer magnets. Their plane is therefore fixed by the direction of the magnetic field in the spectrometer magnets. The design principles and considerations on operational aspects are given in [12].

A complete summary of the crossing angles and the parallel separation in the four interaction points is given in Tabs. 4.2 to 4.5.

Table 4.3: Crossing angle and orbit at IP5 for Beam 1 (half the total beam separation). The minimum separation between Beam 1 and Beam 2 is specified for one plane. The state 'Injection' refers to the optics configuration during injection, 'Ramp' to the configuration during ramp, 'Pre-Collision' to the optics at the end of the ramp but before the low-β squeeze and 'Collision' to the optics configuration at top energy after the low-β squeeze.

State	$\beta^*_{x,y}$ (m)	horizontal crossing angle (μrad)	vertical orbit (mm)	$d_{\rm ip}$ (σ)	$d_{\rm min}$ (σ)
Injection	18.0	+ 160.0	+ 2.50	13.3	10.5
Ramp	18.0	+ 40.0	+ 0.625	13.3	10.5
Pre-collision	0.55	+ 142.5	+ 0.50	60	6.9
Collision	0.55	+ 142.5	+ 0.0	0.0	6.9

Table 4.4: Vertical crossing angle and horizontal orbit at IP2 for Beam 1 (half the total beam separation). Minimum separation between Beam 1 and Beam 2 is specified for one plane.

State	SPEC (ALICE) (μrad)	$\beta^*_{x,y}$ (m)	half external angle $\alpha_{\rm ext}$ (μrad)	half crossing angle α (μrad)	horizontal orbit separation (mm)	$d_{\rm ip}$ (σ)	$d_{\rm min}$ (σ)
Injection	0.0	10.0	$\pm$ 170.0	$\pm$ 170.0	+ 2.00	14.3	9.1
Injection	+ 70.0	10.0	+ 170.0	+ 240.0	+ 2.00	14.3	9.1
Injection	- 70.0	10.0	- 170.0	- 240.0	+ 2.00	14.3	9.1
Collision	+ 70.0	10.0	+ 80.0	+ 150.0	0.18	5	14.8
Collision	- 70.0	10.0	- 80.0	- 150.0	0.18	5	14.8

Table 4.5: Horizontal crossing angle and vertical orbit at IP8 for Beam 1 (half the total beam separation). Minimum separation between Beam 1 and Beam 2 is specified for one plane [a] at one unique position, everywhere else above 20 σ.

State	SPEC (LHCb) (μrad)	$\beta^*_{x,y}$ (m)	half external angle $\alpha_{\rm ext}$ (μrad)	half crossing angle α (μrad)	horizontal orbit separation (mm)	$d_{\rm ip}$ (σ)	$d_{\rm min}$ (σ)
Injection	0.0	10.0	- 170.0	- 170.0	- 2.00	14.3	9.0
Injection	+ 135.0	10.0	- 170.0	- 35.0	- 2.00	14.3	9.0
Injection	- 135.0	10.0	- 165.0	- 300.0	- 2.00	14.3	8.8
Collision	+ 135.0	10.0	- 210.0	- 75.0	0.0	-	6.5 [a]
Collision	- 135.0	10.0	- 65.0	- 200.0	0.0	-	12.8

4.2.2 The high luminosity insertions IR1 and IR5

The high luminosity insertions IR1 (ATLAS) and IR5 (CMS) house the main p-p experiments of the LHC and are identical in terms of hardware and optics, with the exception of the crossing plane, which was chosen vertical in IR1 and horizontal in IR5.

Optics goals

The optics design in IR1/5 is guided by two main requirements:

1. It must provide a range of accessible β^* values (18 m for the injection and 0.55 m for the collision optics) while keeping the total phase advance over the IR constant.
2. In order to have control over the beam size, the beam separation and the nonlinear chromaticity during the change from injection to collision optics, the quadrupole gradients must change smoothly with varying β^* (e.g. the slope of the quadrupole gradient versus time should not change its sign).

Hardware constraints

1. At the IP, the two rings of the LHC share the same vacuum chamber and the same low-beta triplet quadrupoles and the optics solutions for Ring 1 and Ring 2 must have the same triplet gradients.
2. The maximum gradients must not exceed the operating values given in Tab. 3.2.
3. The minimum gradient of the unipolar insertion quadrupoles at injection energy must be larger than 3% of the nominal gradient.
4. The overall beam size must be small enough to fit into the tight aperture of the LHC. The aperture of the insertions is limited by the crossing-angle separation orbit and the beam screen which is installed in all of the insertion region magnets.

Injection optics

At injection, the optics are detuned with a β^* of 18 m (see Fig. 4.5(a) and 4.5(b)). The phase advances across the IR, i.e. from Q13 left to Q13 right from the IP, are the same for both beams and equal to $\mu_x/2\pi = 2.618$ and $\mu_y/2\pi = 2.644$. They are kept constant along the ramp and are increased by $\Delta\mu_x/2\pi = 0.015$ and $\Delta\mu_y/2\pi = 0.005$ just before the squeeze in order to change from the injection tunes ($Q_{x,y} = 64.28/59.31$) to the collision tunes ($Q_{x,y} = 64.31/59.32$).
The recent implementation of beam-screens in the matching section quadrupoles [13] has reduced the mechanical aperture to $n_1 = 6.6 - 6.7$ at a few locations in the insertion which may require tighter mechanical tolerances and/or more frequent re-alignment of the most critical magnets in order to recover the intial IR tunability of $\Delta\mu_x/2\pi \sim 0.1$ and $\Delta\mu_y/2\pi \sim 0.2$ [14] (a detailed definition of n_1 can be found in Sec 4.3). The smallest aperture now occurs at Q5 for Beam 2 in IR1, see Fig. 4.8(a).
The crossing scheme, vertical in IR1 and horizontal IR5 is shown in Fig. 4.6. The sign of the vertical crossing angle in IR1 ($\theta_c = \pm 160\,\mu$rad) and of the vertical separation in IR5 ($\Delta y = \pm 2.5$ mm) can be chosen arbitrarily. On the other hand, due to the ring geometry (Beam 1 internal in sectors 4-5 and 7-8) and in order to maximise the beam-beam separation at injection, the (horizontal) parallel separation bump must be negative for Beam 1 in IR1 ($\Delta x = -2.5$ mm) and its (horizontal) crossing angle has to be positive at IP5 ($\theta_c = +160\,\mu$rad).

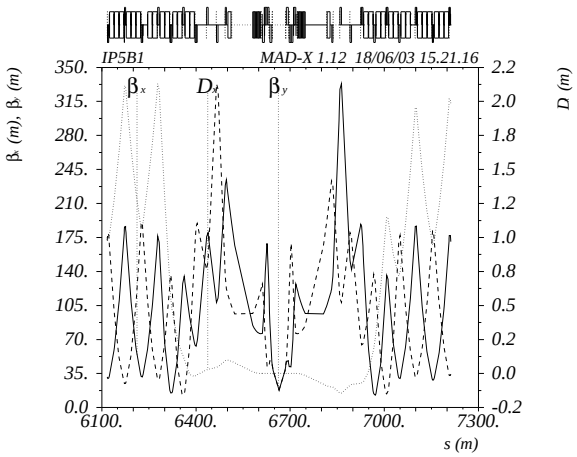

(a) Beam 1, injection optics

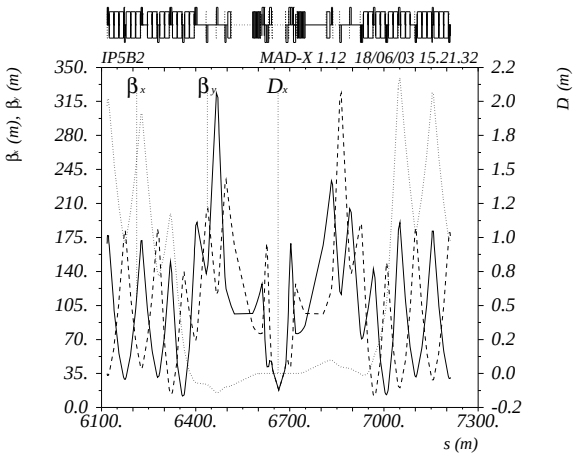

(b) Beam 2, injection optics

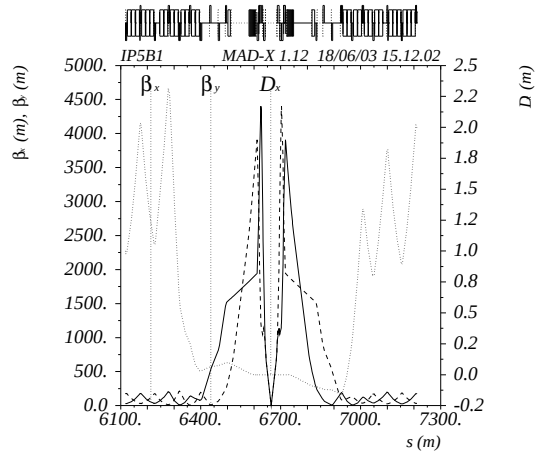

(c) Beam 1, collision optics

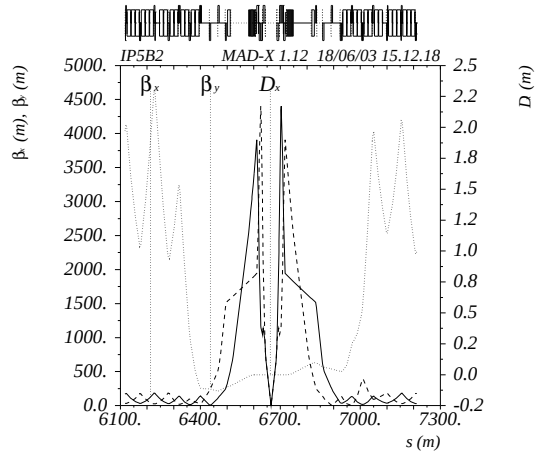

(d) Beam 2, collision optics

Figure 4.5: Injection (top) and collision (bottom) optics of the high-luminosity insertions at IP1 and IP5 for a β^* of 18 m and 0.55 m.

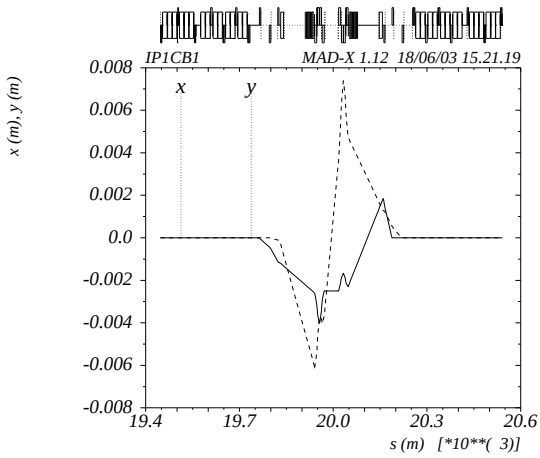

(a) Beam 1 in IR1

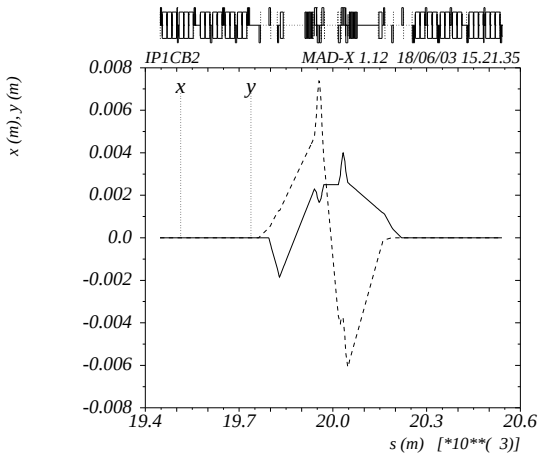

(b) Beam 2 in IR1

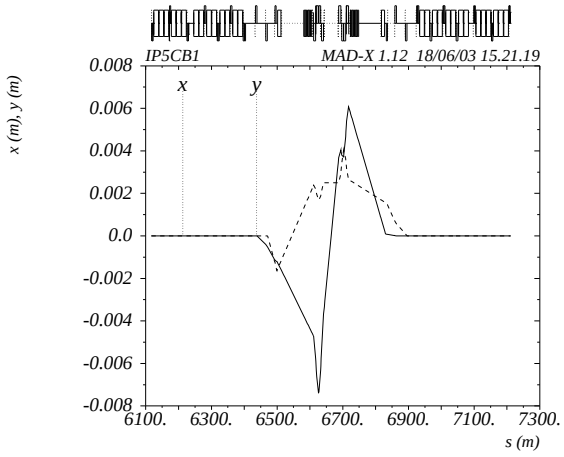

(c) Beam 1 in IR5

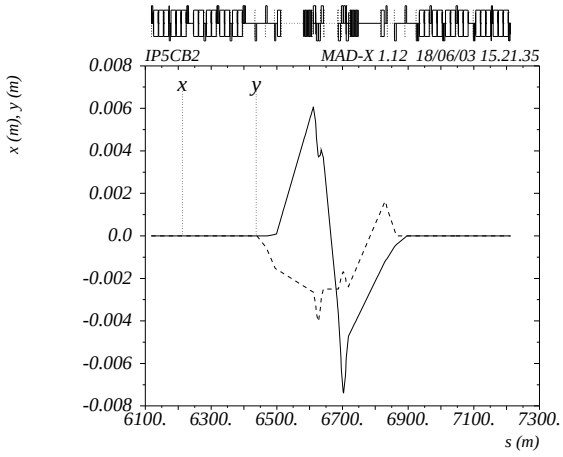

(d) Beam 2 in IR5

Figure 4.6: Crossing scheme for Beam 1 and Beam 2 at injection for the high-luminosity insertions IR1 (top) and IR5 (bottom).

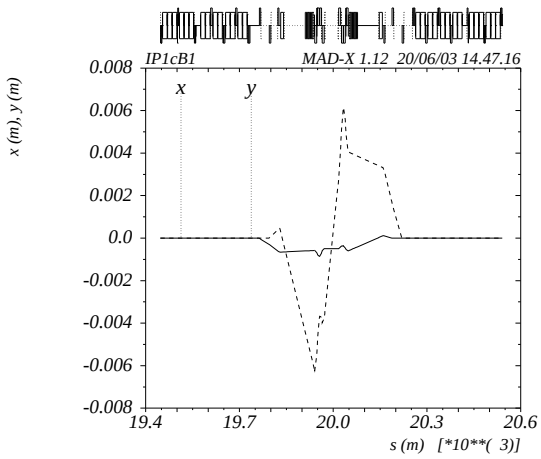

(a) Beam 1 in IR1

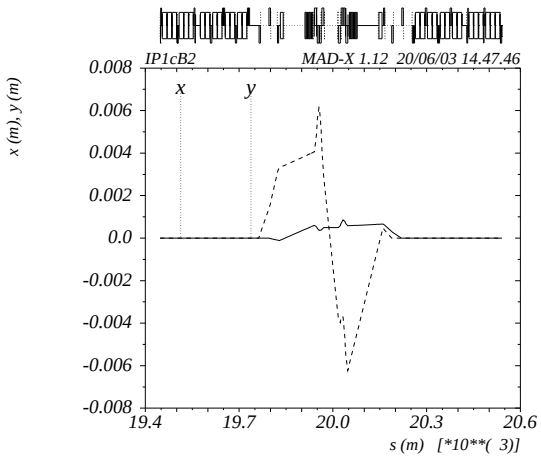

(b) Beam 2 in IR1

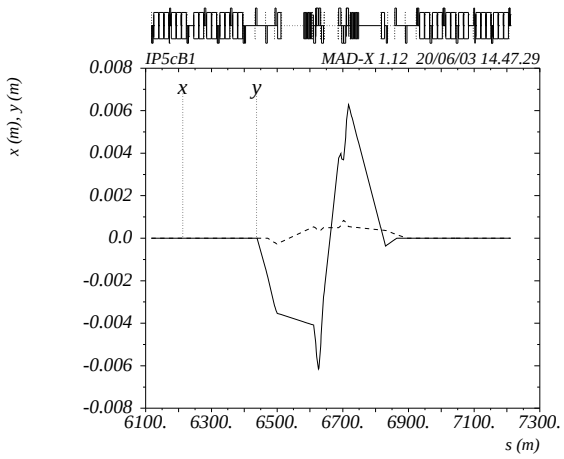

(c) Beam 1 in IR5

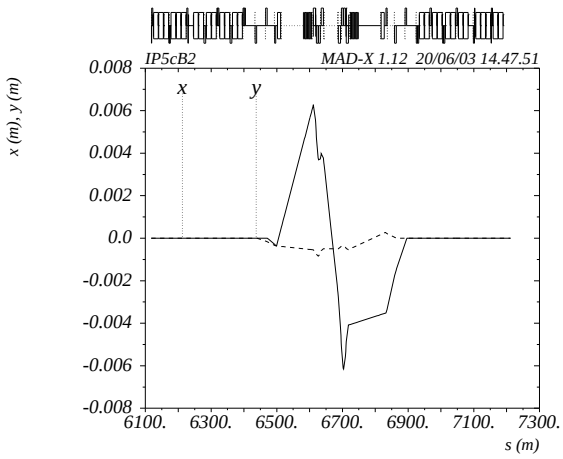

(d) Beam 2 in IR5

Figure 4.7: Crossing scheme for Beam 1 and Beam 2 in pre-collision for the high-luminosity insertions IR1 (top) and IR5 (bottom); IP is assumed to be shifted transversally by $\Delta y = -0.5$ mm in IR1 and $\Delta x = 0.5$ mm in IR5.

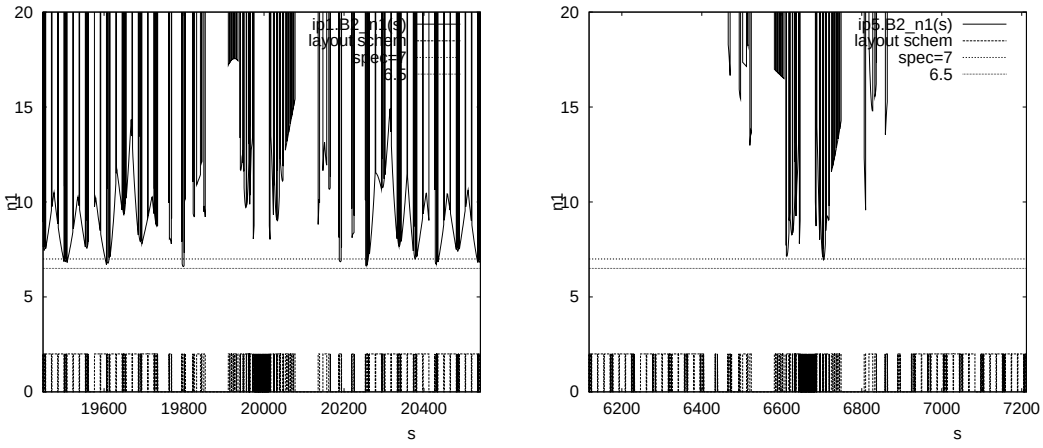

Figure 4.8: Typical figures for the mechanical acceptance of the high-luminosity insertions IR1 and IR5 expressed in terms of n_1 at 450 GeV (injection optics) (left) and 7 TeV (pre-collision optics) (right).

Collision optics

The collision optics of IR1 and IR5 is shown in Fig. 4.5(c) and 4.5(d) for a β^* of 0.55 m. In order to maximise the mechanical acceptance of the low-β quadrupoles, the interaction point can be shifted transversally, that is in the crossing plane, by $\Delta y = -0.5$ mm in IR1 and $\Delta x = 0.5$ mm in IR5, resulting in a net increase of the triplet aperture by $\Delta n_1 = 0.4$. As a result, in spite of the recent implementation of beam-screens in the low-β quadrupoles [13], the specification of $n_1 = 7$ can be met for both beams and both insertions (worst case obtained for Beam 2 in IR5 with $n_1 = 6.98$, see Fig. 4.8(b)).

The crossing schemes in IR1 and IR5 are shown in Fig. 4.7 for the pre-collision optics, i.e. collision optics with a half-parallel separation and crossing angle of ± 0.5 mm and $\pm 150\,\mu$rad, respectively. The crossing schemes ensure an average beam-beam separation of 9.4 σ over the IR, with a minimum separation of 6.6 σ inside the triplet assembly.

4.2.3 IR2

IR2 houses the ALICE experiment and the injection elements for Beam 1.

Optics goals

The optics design in IR2 is guided by three main requirements:

1. It must provide a range of accessible β^* values (0.5 m $< \beta^* <$ 50 m) while keeping the total phase advance over the IR constant.

2. The Ring 1 optics must satisfy the requirements imposed by the beam injection and provide a vertical phase advance of 90° between MKI and TDI, and a vertical phase advance of $(360^\circ - 20^\circ)$ and $(360^\circ + 20^\circ)$ between the TDI and the two auxiliary collimators. [2]

3. In order to have control over the beam sizes, the beam separation and the non-linear chromaticity during the change from injection to collision optics the quadrupole gradients must change smoothly with varying β^* (e.g. the slope of the quadrupole gradient versus time should not change its sign).

[2]The auxiliary collimators are incompatible with the space requirements for the DFB installation in the LHC lattice version V6.4. The TCL implementation is being revised for V6.5.

Hardware constraints

1. At the IP, the two rings of the LHC share the same vacuum chamber and the same low-beta triplet quadrupoles and the optics solutions for Ring 1 and Ring 2 must have the same triplet gradients.

2. The maximum gradients must not exceed the operating values given in Tab. 3.3

3. The minimum gradient of the unipolar insertion quadrupoles at injection energy must be larger than 3% of the nominal gradient.

4. The overall beam size must be small enough to fit into the tight aperture of the LHC. The aperture of the insertions is limited by the beam screen and the crossing-angle separation orbit. All magnets of the insertions are equipped with a beam screen.

5. For the large β^* optics the maximum achievable crossing angle is limited by the available orbit corrector strength. In fact, the orbit corrector strength limits the maximum acceptable β^* value in IR2 ($\beta^* \leq 50$ m).

Injection optics

At injection, the β^* value is determined by the injection constraints [15] which imply an optics with $\beta^* = 10$ m. Figs. 4.10(a) and 4.10(b) show the corresponding optics functions for Beam 1 and Beam 2, respectively. The phase advances across the IR (i.e. from Q13 left to Q13 right) are the same for both beams and equal to $\mu_x/2\pi = 2.991$ and $\mu_y/2\pi = 2.844$. The recent implementations of beam-screens in the matching section quadrupoles [13], and the optimisation of the DFB length [16] with the implied repositioning of the Q6 quadrupole magnets and the shift of the Q3 triplet quadrupole magnet position [1], has reduced the mechanical aperture with respect to the V6.0 solution presented in [15]. While the solutions presented in [15] had apertures larger than $n_1 = 7$ in all positions of the insertion it now drops to minimum values between $n_1 = 6.6 - 6.7$ at a few locations in the insertion. This may require tighter mechanical tolerances and/or more frequent re-alignment of the most critical magnets (a detailed definition of n_1 can be found in Sec. 4.3). The optics presented in Fig. 4.10(b) recuperated some of the aperture loss in Q6 by allowing larger than nominal optic functions at Q8 and relaxing the vertical phase advance constraints for the auxiliary collimators implying a further optimization of the auxiliary collimator positions. The vertical phase advance between the MKI and TDI is kept at 90°. This approach yields a minimum aperture of $n_1 = 6.68$ at Q6 and $n_1 = 6.71$ at Q8. Under this condition a large fraction of the IR tunability quoted in [15] is lost due to the reduced mechanical aperture imposed by the beam screen.
The crossing scheme, vertical crossing angle and a parallel separation in the horizontal plane is shown in Fig. 4.11. The sign of the vertical separation can be chosen arbitrarily. On the other hand, due to the ring geometry and in order to maximize the beam-beam separation at injection, the (horizontal) parallel separation bump must be positive for Beam 1 and negative for Beam 2.

Collision optics

The ALICE luminosity during proton beam operation assumes $\beta^* = 10$ m (equivalent to the injection optics) with a transverse beam separation of 5 σ. Because of the reduced beam size at 7 TeV there is no aperture problem for this configuration.

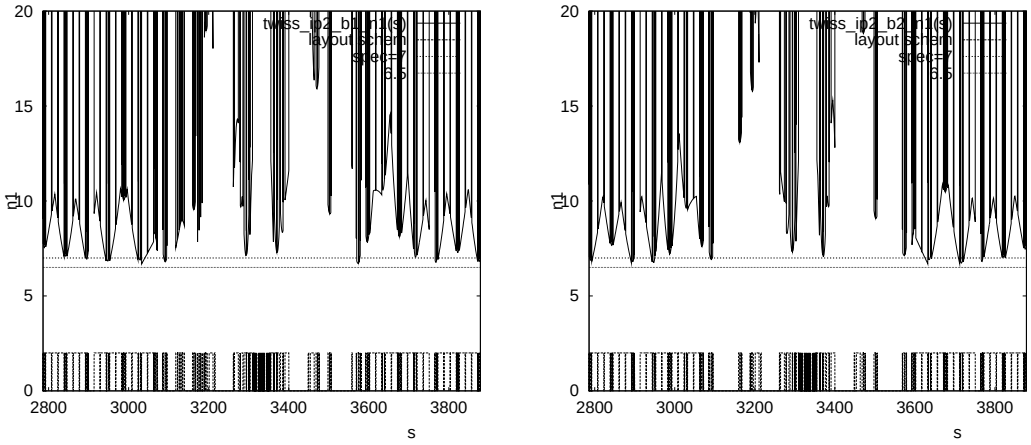

Figure 4.9: The mechanical acceptance in IR2 expressed in terms of n_1 at 450 GeV (injection optics) for Beam 1 (left) and Beam 2 (right). The minimum acceptance of $n_1 = 6.68$ occurs for Beam 1 in Q6.R2 and Q8.L2.

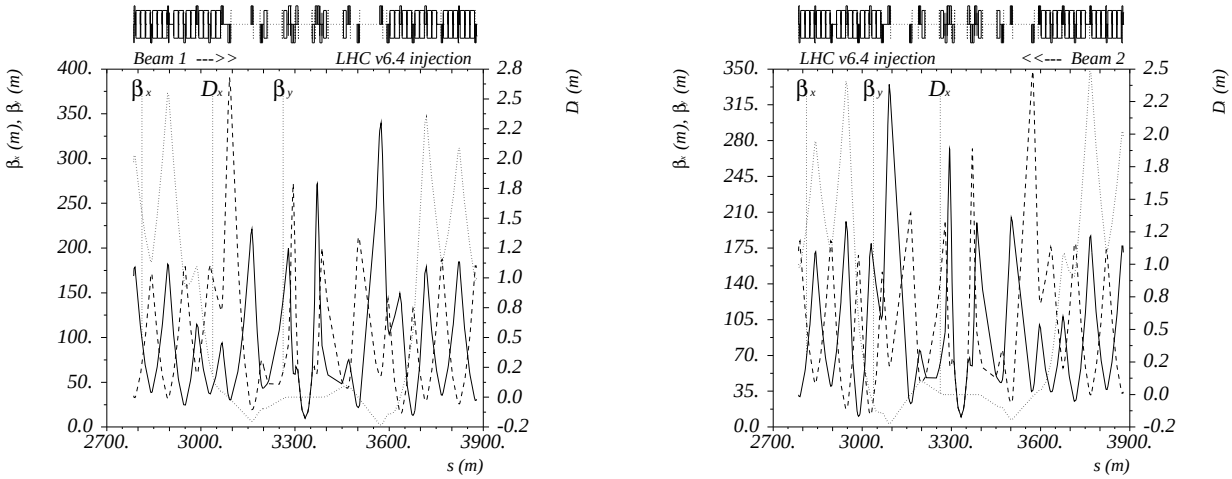

Figure 4.10: Injection (top) ($\beta^* = 10.0$ m) optics in IR2 for Beam 1 (left) and Beam 2 (right).

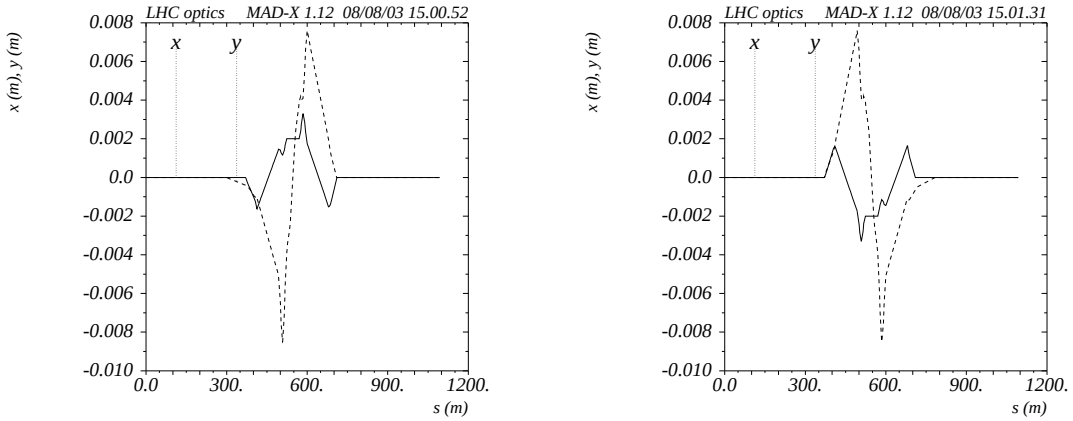

Figure 4.11: Crossing scheme for Beam 1 (left) and Beam 2 (right) at injection for IR2.

4.2.4 IR3

Insertion IR3 houses the Momentum Collimation system. The momentum range of the *nominal* circulating beam does not exceed $\pm 1\ 10^{-3}$. Particles outside this range must be absorbed in the momentum cleaning insertion before they can be lost in the arcs. This is done using a multi turn two stage collimation system (see Chap 18 for more details on the collimation system design). In order to decouple the momentum collimation in IR3 from the betatron-collimation in IR7, the primary collimator jaws in IR3 must be at a location with large dispersion and small betatron function. The optics design in IR3 therefore aims at maximizing the normalized dispersion:

$$\eta_{\rm D} = \frac{D_x}{\sqrt{\beta_x}}. \tag{4.1}$$

In order to protect the arc aperture from off momentum particle losses the normalized dispersion at the primary collimator must satisfy [17]:

$$\eta_{\rm D,prim}(n_1) \geq \frac{n_1\,\eta_{\rm D,arc}}{A_{\rm arc,inj}(\delta_p = 0) - (n_2^2 - n_1^2)^{1/2}} = 0.185\ {\rm m}^{1/2} \tag{4.2}$$

where $A_{\rm arc,inj}(\delta_p = 0)$ is the arc aperture for on-momentum particles ($A_{\rm arc,inj}(\delta_p = 0) = 12$), $\eta_{\rm D,arc} = 0.205\ {\rm m}^{1/2}$ with errors in the focusing quadrupole magnets (without errors one has $\eta_{\rm D,arc} = 0.16\ {\rm m}^{1/2}$). (See Sec 4.3 for more details.) n_1 and n_2 are the apertures of the primary and secondary collimator jaws in multiples of the RMS beam size ($n_1 = 7$ and $n_2 = 7n_1/6 = 8.2$) (a detailed definition of n_1 can be found in Sec 4.3). Requiring further that the cut of the secondary halo is independent of the particle momentum one obtains a second constraint for the optics at the position of the primary collimator [17, 18, 19, 20]:

$$\frac{D_x'}{D_x} = -\frac{\alpha_x}{\beta_x}. \tag{4.3}$$

Satisfying the constraints (4.2) and (4.3) can be facilitated by choosing convenient locations for the primary collimator jaws in the insertion. However, once the locations of the primary collimator jaw are fixed the positions of the secondary collimator jaws are constrained by the required phase advance between primary and secondary collimators. At least four secondary jaws are required to cut the secondary halo adequately [19] and it has been shown that six jaws offer a substantial further improvement [21]. The V6.4 layout features six secondary collimator jaws per beam. As the cleaning insertion provides only a limited range of acceptable positions for the secondary collimator jaws, the request for a given set of phase advances between the collimator jaws drastically limits the range of accessible optics solutions. Furthermore, the above constraints must be satisfied simultaneously for both beams.

The V6.4 optics solution shown in Fig. 4.12 provides a normalized dispersion value of $0.21\ {\rm m}^{1/2}$ at insertion quadrupole Q5 upstream of the IP. The primary collimator is located at the upstream side of the insertion between Q5 and Q6 [22][21]. This value is larger than the requested value in (4.2) and still provides some margin for optics errors. The total betatron phase advances in the normal conducting region available for the primary and secondary collimators are $0.5 * 2\pi$ and $0.2 * 2\pi$ in the horizontal and vertical plane respectively.

The optics in Fig. 4.12 shows a flat peak in the normalized dispersion function at the primary collimator. This provides efficient collimation over a large momentum error range [18]. This optical feature was obtained by moving Q6 closer to the IP and is the reason why the distance between the two groups of MBWs in IR3 is shorter than that in IR7.

Fig 4.15 shows the aperture of the insertion for Beam 1 in terms of the required primary collimator opening. One clearly recognizes the effect of the large dispersion near Q5 where the minimum aperture reaches a value of $n_1 = 5.5$. This is not problematic as long as the momentum collimators are in operation, because the primary betatronic amplitude cut at the edge of the bucket is $\approx 4\sigma$, see Fig. 4.13. At top energy, the normalized primary collimator aperture can be increased. While the dispersion function does not change with the beam energy, the betatronic beam size shrinks inversely with the square root of the beam energy allowing operation with a larger n_1 (see Fig. 4.14).

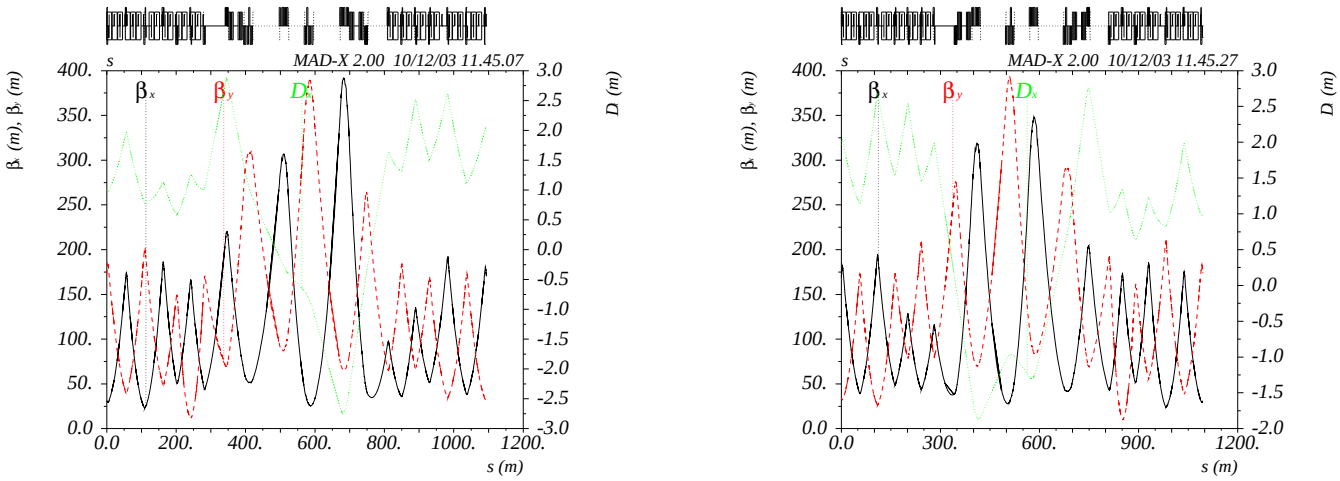

Figure 4.12: β functions and normalized dispersion $D_x/\sqrt{\beta_x}$ in IR3 for Beam 1(left) and Beam 2 (right). The optics corresponds to the new V6.5 layout.

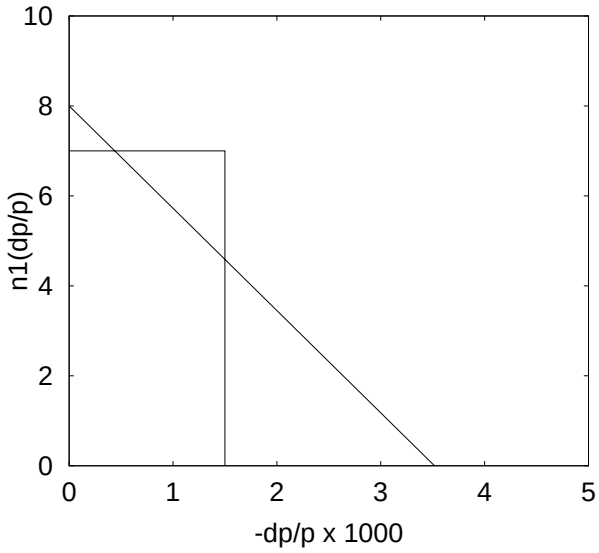

Figure 4.13: The betatron primary aperture as a function of the momentum as cut by the primary momentum collimator at injection, see text. Particles which drift beyond the line are captured and absorbed. The rectangle indicates the space occupied by circulating particles which are inside the bunch and which have an amplitude smaller than the cut made by the betatron collimation.

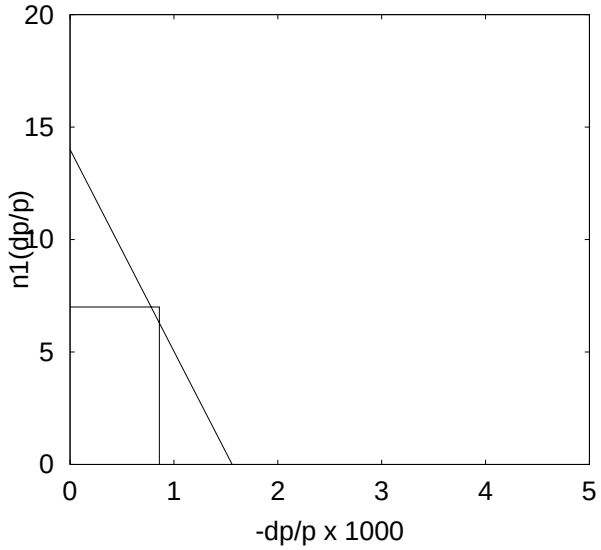

Figure 4.14: The betatron primary aperture as a function of the momentum as cut by the primary momentum collimator at top energy, see text and Fig. 4.13 for a description of the content.

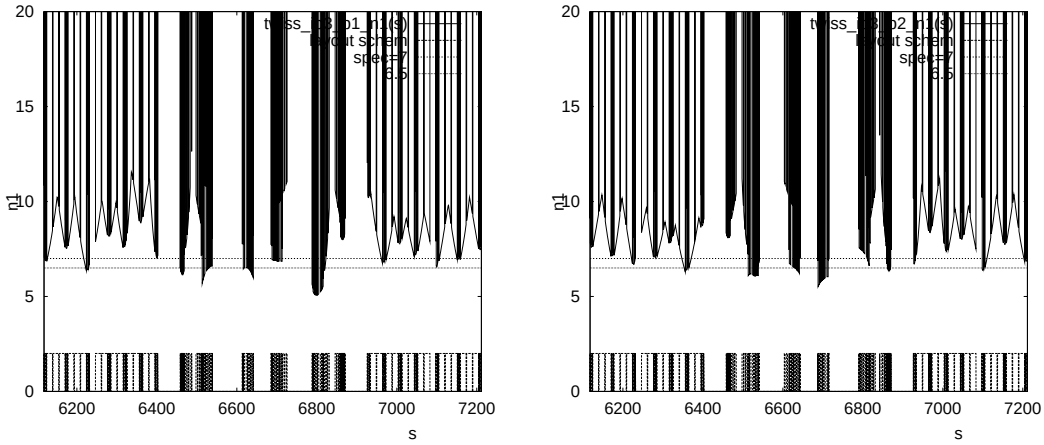

Figure 4.15: The normalized primary aperture plot in IR3 for Beam 1 (left) and Beam 2 (right). The reduced aperture at Q5 at the down stream side of the IP is caused by the increased dispersion. The aperture corresponds to the new V6.5 optics and layout.

4.2.5 IR4

IR4 houses the RF and feed-back systems as well as some of the LHC beam instrumentation. None of these systems impose serious constraints on the optics thus allowing a range of optics solutions with different phase advances for IR4. For this reason IR4 could be used to adjust the phase advances between IR1 and IR5 and to adjusts the tunes if the global LHC optics is constrained [23][24] (and see Sec. 4.6.2). However, the introduction of beam screens in all insertion regions imposes a strong aperture limitation that essentially removes the flexibility of the insertion optics that was available in previous optics versions. In fact the aperture limitation generated by the beam screens is so strong that several insertions can now no longer satisfy the intial goals of an aperture with $n_1 \geq 7$ (see Sec. 4.3 for a description of n_1).

The matching in IR4 is done using all quadrupoles at the same time while constraining the maximum β-function in the dispersion suppressors (from Q7 to Q11) to the maximum value in the LHC arcs. The maximum β-function in the long straight section is limited to 600 m at Q5 and Q6 on both sides of the IP. The horizontal dispersion is matched to zero in the cavities.

Fig. 4.16 shows the optics functions for Beam1 in IR4 and Fig. 4.17 the range of accessible phase advances over IR4 for the case without beam screens in the insertion magnets. The decision to place beam screens inside all insertion magnets lowers the available mechanical aperture in IR4 and thus the accessible range of phase advances over the insertion.

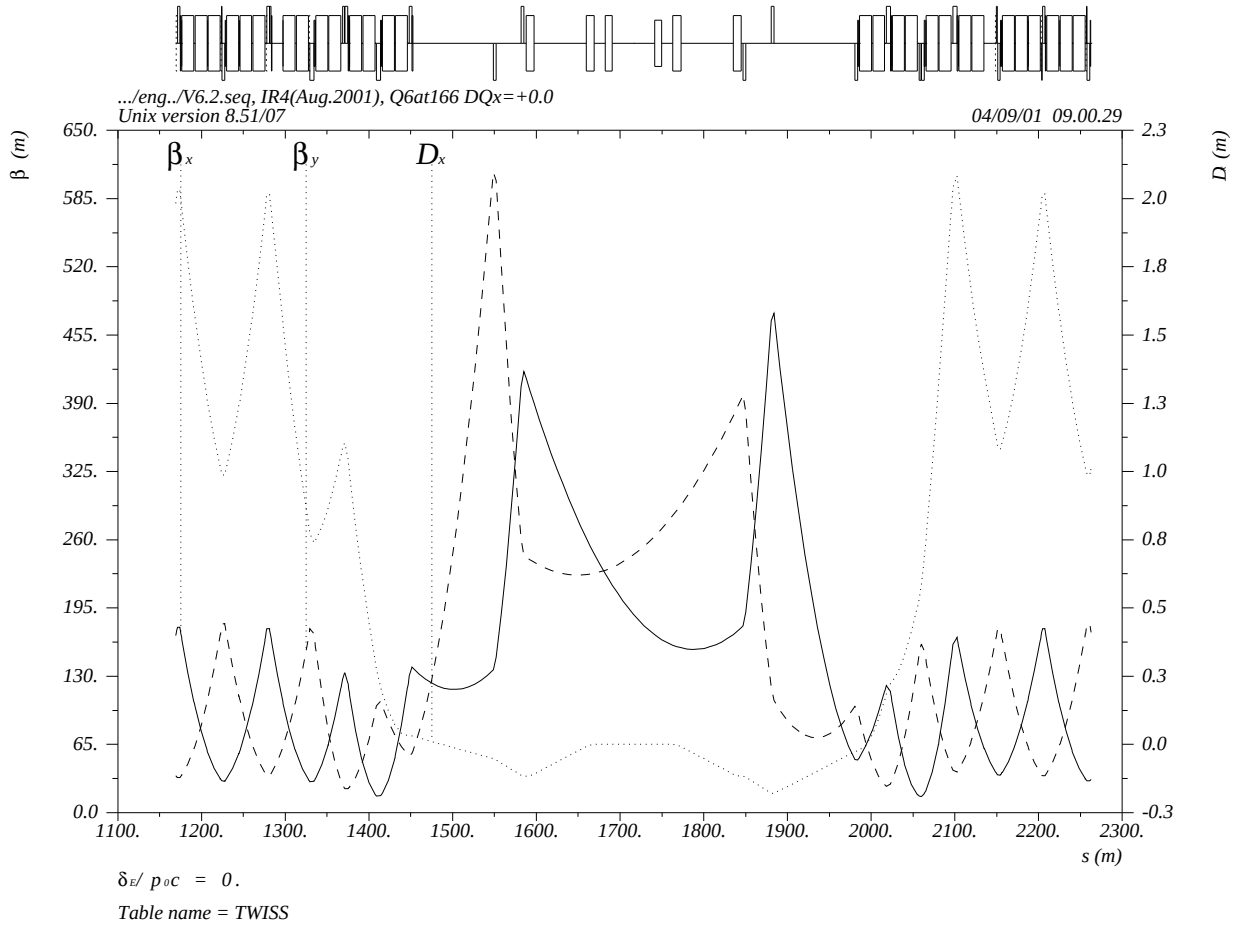

Figure 4.16: The optics functions for Beam 1 in IR4.

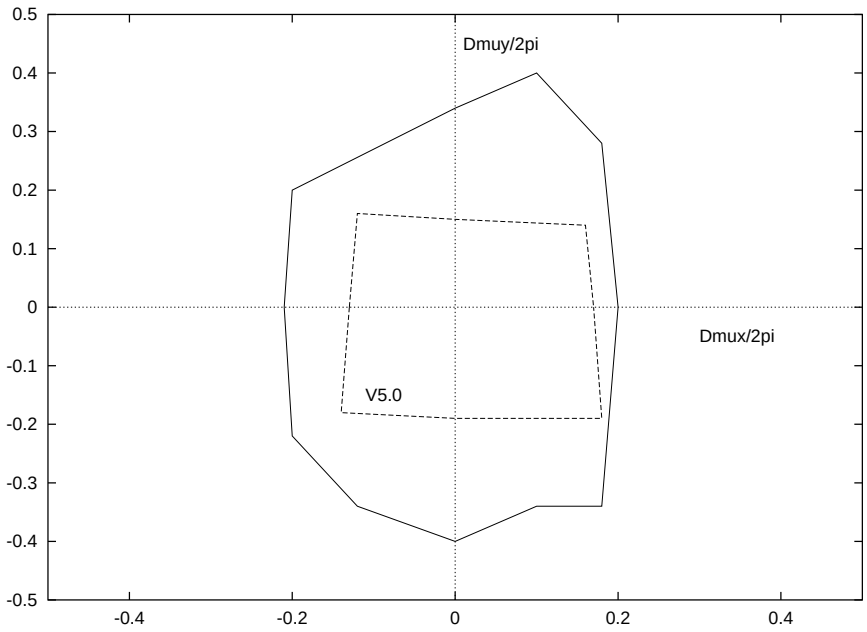

Figure 4.17: Outer figure: possible variations of the phase advance in IR4 without beam screens in the insertion magnets. The inner figure shows the same variation obtained with the old design.

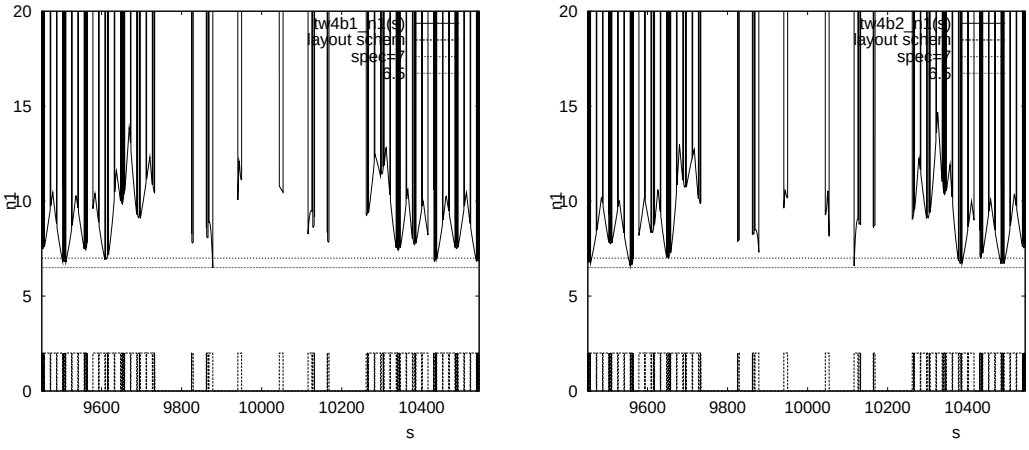

Figure 4.18: The mechanical acceptance in IR4 expressed in terms of n_1 at 450 GeV (injection optics). The minimum acceptance of $n_1 = 6.5$ occurs for Beam 1 and Beam 2 in the D4 dogleg dipole magnet (a detailed definition of n_1 can be found in Sec. 4.3).

4.2.6 IR6

IR6 houses the beam abort systems for Beam 1 and Beam 2. The optics in IR6 is constraind by the maximum aperture of the insertion quadrupole and septum magnets. The aperture constraint can be satisfied for a range of optics solutions. However, the introduction of beam screens in all insertion regions imposes a strong aperture limitation that essentially removes the flexibility of the insertion optics that was available in previous optics versions. Fig. 4.19 shows the optics functions for Beam1 in IR6 and Fig. 4.20 the range of accessible phase advances over IR6. Actually it is possible to change the phases by even larger amounts than indicated in 4.20 in a discontinuous way. This is discussed in [25]. However, it should be noted here that the tuneability in Fig. 4.20 was established under the assumption that the insertion magnets in IR6 are not equipped with beam screens. The decision to place beam screens inside all insertion magnets lowers the available mechanical aperture in IR6 and thus the accessible range of phase advances over the insertion.

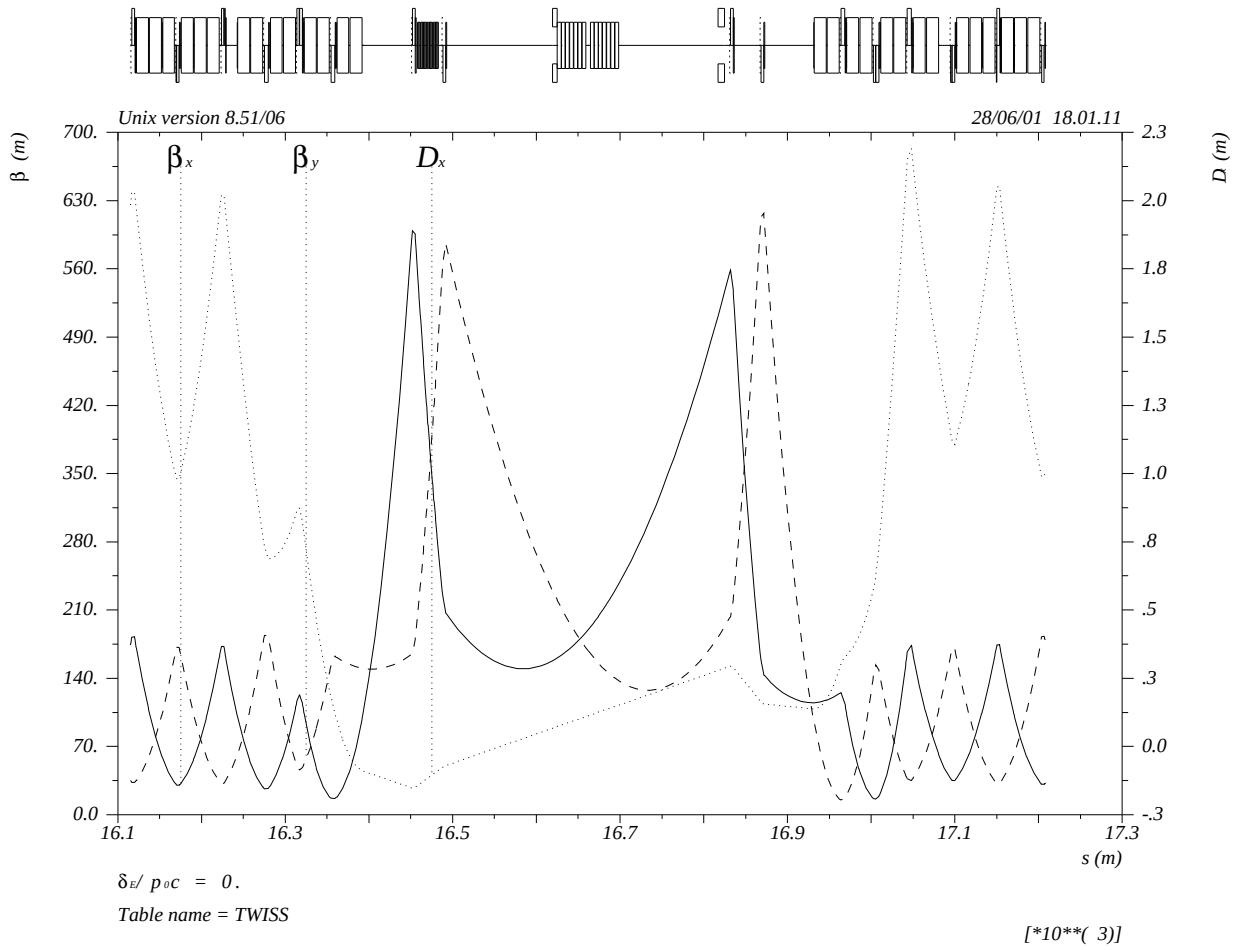

Figure 4.19: The optics functions for Beam 1 in IR6.

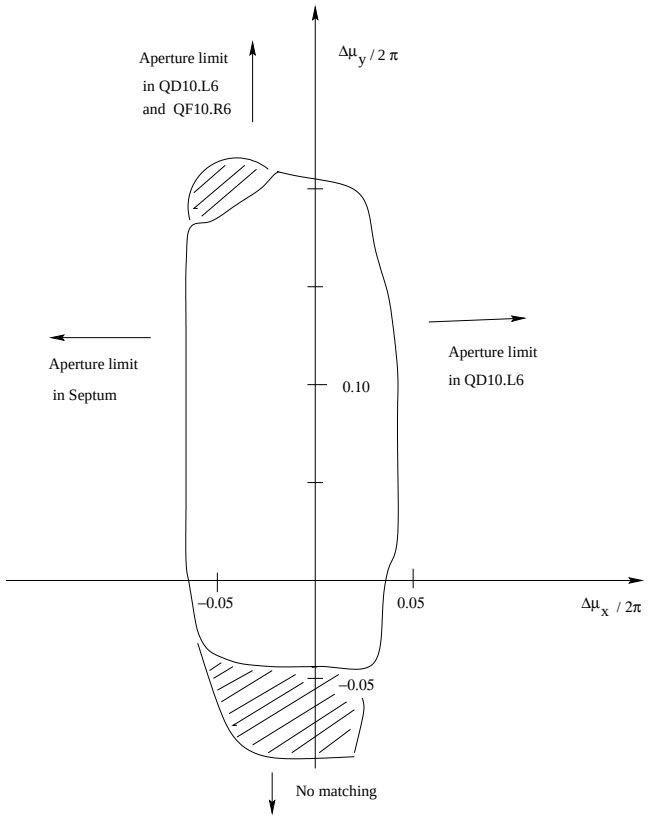

Figure 4.20: The range of accessible phase advances over IR6.

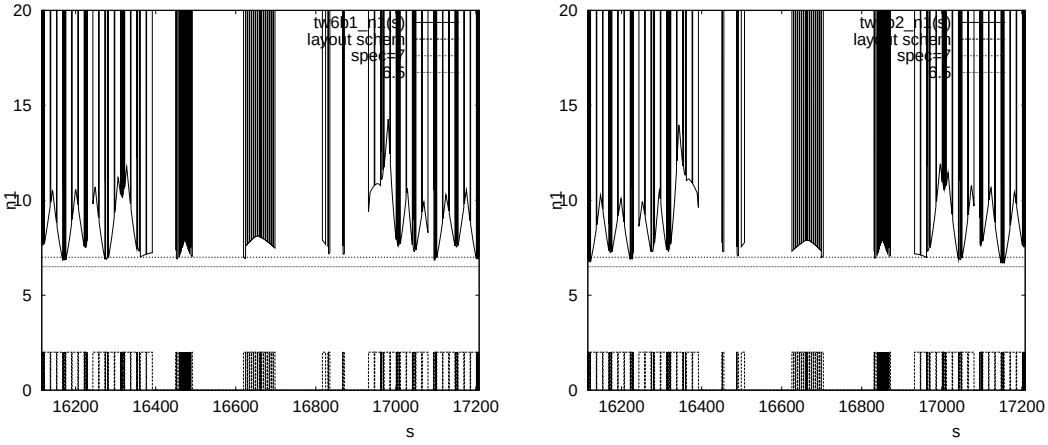

Figure 4.21: The mechanical acceptance in IR6 expressed in terms of n_1 at 450 GeV (injection optics). The minimum acceptance of $n_1 = 6.7$ occurs for Beam 2 inside the DS (a detailed definition of n_1 can be found in Sec. 4.3).

4.2.7 IR7

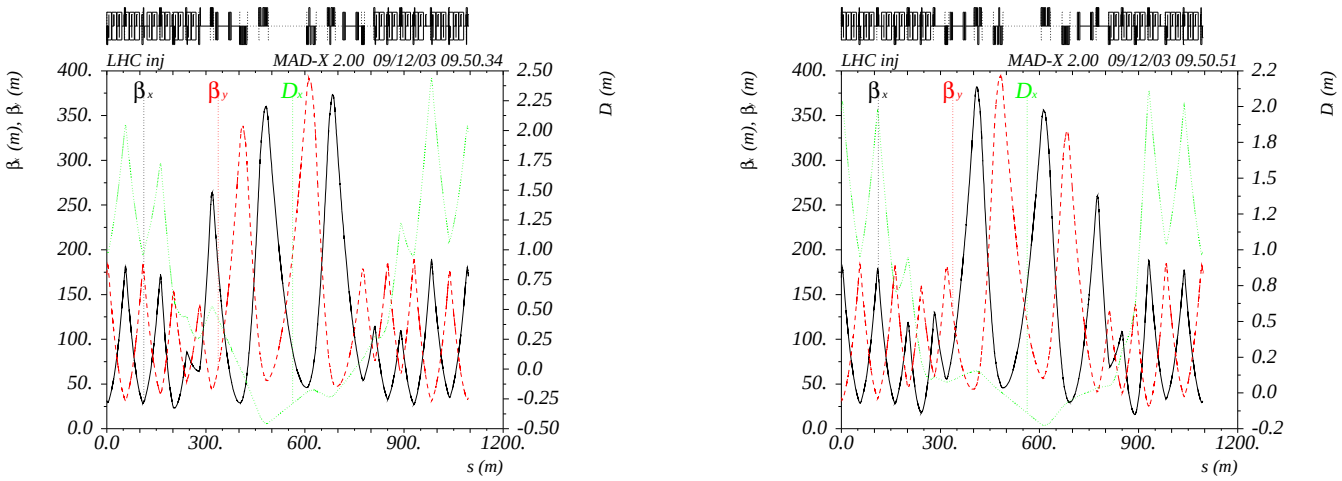

(a) Beam 1 (b) Beam 2

Figure 4.22: Lattice functions in IR7. The optics corresponds to the new V6.5 layout.

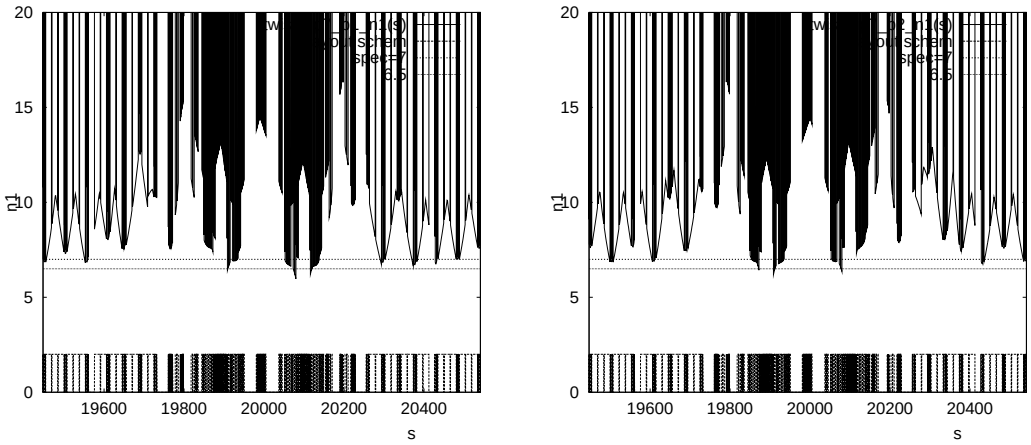

Figure 4.23: The normalized primary aperture plot in IR7 for Beam 1 (left) and Beam 2 (right). The plots correspond to the new V6.5 optics and layout.

Insertion IR7 houses the Betatron Collimation system. The dispersion function in the long straight section between Q7L and Q7R is kept small, in order to reduce the effect of the off-momentum motion on the collimation. The primary collimators are located at the upstream side of the IP, between Q5 and Q6. The total betatron phase advances in the normal conducting region of the insertion are $0.5 * 2\pi$ and $0.4 * 2\pi$ in the horizontal and vertical plane respectively. The primary betatron cleaning is made with three primary jaws, namely horizontal, vertical and skew. A detailed derivation for an ideal optics is found in [18, 19]. A reasonably good optimum is obtained with four secondary jaws per primary collimator. As the apertures of the LHC magnets in general have non-rectangular cross sections, collimation and aperture studies must take into account the combined horizontal and vertical particle motion. In this respect a problem arises for particles having large amplitudes in both transverse planes, because they can still escape through a series of collimators if the phases of their H and V betatron oscillations differ by 90 or 270° [26]. These particles may be lost outside the collimation region, at locations where the horizontal and vertical oscillations of the particles are again in phase. This problem is particularly severe if all collimators have approximately the same difference between the horizontal and vertical

betatron phases. Introducing fluctuations for $\mu_y - \mu_x$ in the region of the collimators reduces the above problem and particles having large amplitudes in both transverse planes are easier to intercept. To this end the minima of the β functions are made small, thus accelerating the phase advance alternatively in the horizontal and vertical planes [27].

In an insertion of finite length, the best correlation of the phase advances can never be reached. The optics was therefore optimized for maximum opening of the secondary collimators. For a fixed optics and given primary collimator opening, the required opening of the secondary collimator jaws is evaluated numerically with the code 'Distribution of Jaws', or DJ [20]. Once an optimum optics is obtained for one beam, a simultaneous matching of the two beams is performed, in order to find a common solution which is as close as possible to the initial solution of the single beam. This procedure typically generates an aperture loss of approximately $0.2\ \sigma$. Fig 4.22 shows the corresponding optics functions in IR7 for Beam 1 and Beam 2. The aperture of IR7 for this optics is shown in Fig 4.23. At some locations the equivalent primary aperture is as low as $n_1 \approx 6.3$ which is clearly smaller than the specified value $n_1 = 7$, see Sec 4.3. However, in warm elements this is still acceptable. It was also checked that the power deposition in the vacuum chamber is acceptable, w.r.t. to mechanical integrity and radiation.

Although the beam sizes, and thus the collimator apertures, decrease with increasing beam energy, the same IR7 optics will be used at all energies.

4.2.8 IR8

IR8 houses the LHCb experiment and the injection elements for Beam 2. It features a special layout where the IP is shifted by 3 half RF wavelengths ($\rightarrow\approx$ 11.25 m) in order to provide enough space in the cavern for the spectrometer magnet. This shift of the IP has to be recuperated before the beam enters back into the dispersion suppressor sections and implies a non-symmetric magnet layout in the matching section.

Optics goals

The optics design in IR8 is guided by three main requirements:

1. It must provide a range of accessible β^* values (1.0 m $< \beta^* <$ 50 m) while keeping the total phase advance over the IR constant.
2. The Ring 2 optics must satisfy the requirements imposed by the beam injection and provide a vertical phase advance of 90° betwen MKI and TDI, and a vertical phase advance of $(360^\circ - 20^\circ)$ and $(360^\circ + 20^\circ)$ between the TDI and the two auxiliary collimators. [3]
3. In order to have control over the beam sizes, the beam separation and the non-linear chromaticity during the change from injection to collision optics the quadrupole gradients must change smoothly with varying β^* (e.g. the slope of the quadrupole gradient versus time should not change its sign).

Hardware constraints

1. At the IP, the two rings of the LHC share the same vacuum chamber and the same low-beta triplet quadrupoles and the optics solutions for Ring 1 and Ring 2 must have the same triplet gradients.
2. The maximum gradients must not exceed the operating values given in Tab. 3.4
3. The minimum gradient of the unipolar insertion quadrupoles at injection energy must be larger than 3% of the nominal gradient.
4. The overall beam size must be small enough to fit into the tight aperture of the LHC. The aperture of the insertions is limited by the crossing-angle separation orbit and the beam screen which is installed in all insertion magnets.

[3] The auxiliary collimators are incompatible with the space requirements for the DFB installation in the LHC lattice version V6.4. The TCL implementation is being revised for V6.5.

5. For the large β^* optics the maximum achievable crossing angle is limited by the available orbit corrector strength. In fact, the orbit corrector strength limits the maximum acceptable β^* value in IR8 to $\beta^* \leq 50$ m.

Injection optics

At injection, the β^* value is determined by the injection constraints [28] which imply a detuned optics with a β^* of 10 m. Fig 4.24(a) and 4.24(b) show the corresponding optics functions for Beam 1 and Beam 2 respectively. The phase advances across the IR (i.e. from Q13 left to Q13 right) are the same for both beams and equal to $\mu_x/2\pi = 3.204$ and $\mu_y/2\pi = 2.804$. The recent decision to install beam-screens in the matching section quadrupoles [13] and the optimization of the DFB length [16] with the implied repositioning of the Q6 quadrupole magnets and the shift of the Q3 triplet quadrupole magnet position [1], have reduced the mechanical aperture with respect to the V6.0 solution presented in [28]. While the solutions presented in [28] had apertures larger than $n_1 = 7$ in all positions of the insertion it now drops to minimum values between $n_1 = 6.6 - 6.7$ at a few locations in the insertion which might require tighter mechanical tolerances and/or more frequent re-alignment of the most critical magnets (a detailed definition of n_1 can be found in Sec. 4.3). The optics presented in Fig 4.24(b) recuperated some of the aperture loss in Q6 by allowing larger than nominal optic funtions at Q12 and relaxing the vertical phase advance constraints for the auxilary collimators. For the V6.4 lattice layout the injection optics provides $(360^\circ - 36^\circ)$ and $(360^\circ + 0.4^\circ)$ for the vertical phase advances between the TDI and the auxilary collimators. These values can be improved by optimizing the positions of the auxilary collimators. Moving the collimator next to Q6 (TCL.6L8.B2) by 3.5 m closer to the Q6 magnet and the collimator next to Q7 (TCL.7L8.B2) by 8 m away from the Q7 magnet provides $(360^\circ - 29^\circ)$ and $(360^\circ + 10^\circ)$ for the vertical phase advances between the TDI and the auxilary collimators. The vertical phase advance between the MKI and TDI is kept at 90°. This approach yields a minimum aperture of $n_1 = 6.65$ at Q6 and $n_1 = 6.68$ at Q12. Under this condition a large fraction of the IR tunability quoted in [28] is lost due to the reduced mechanical aperture imposed by the beam screen.

The crossing scheme, horizontal crossing angle and a parallel separation in the vertical plane is shown in Fig. 4.25. The sign of the vertical separation can be chosen arbitrarily. On the other hand, due to the ring geometry and in order to maximise the beam-beam separation at injection, the (horizontal) crossing angle bump must be negative for Beam 1 and positive for Beam 2. Depending on the polarity of the LHCb spectrometer magnet this implies either partial compensation or addition of the two crossing angle contributions coming from the external crossing angle separation orbit bump and the spectrometer compensation bump.

Collision optics

Fig 4.24(c) shows the collision optics with $\beta^* = 1.0$ m. The crossing scheme in IR8 is shown in Fig 4.26. Fig 4.27 shows the mechanical acceptance in IR8 for the injection and $\beta^* = 1.0$ m collision optics.

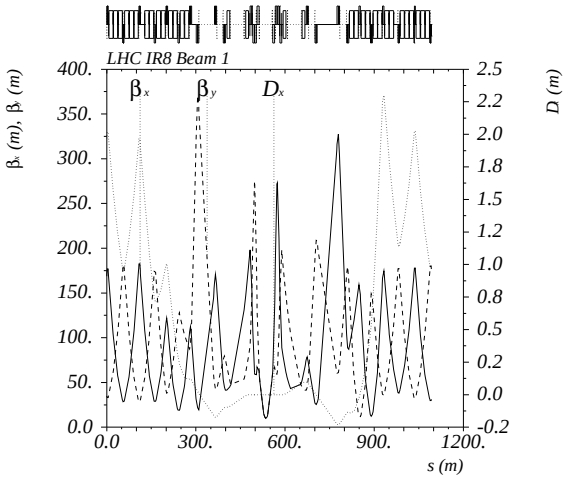

(a) Beam 1, injection optics

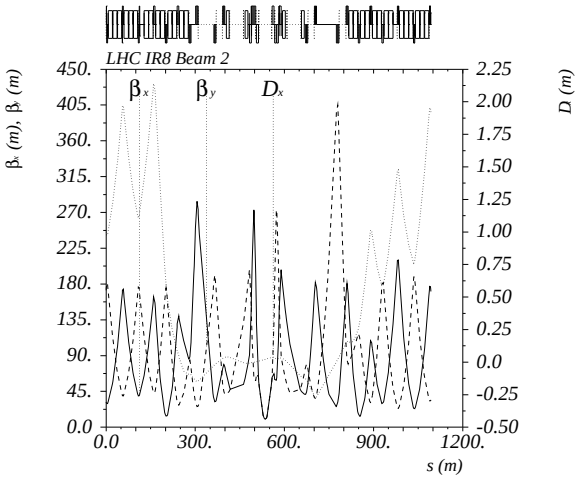

(b) Beam 2, injection optics

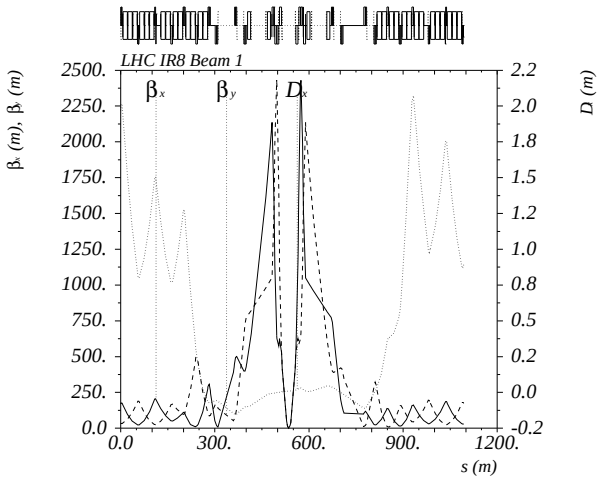

(c) Beam 1, collision optics

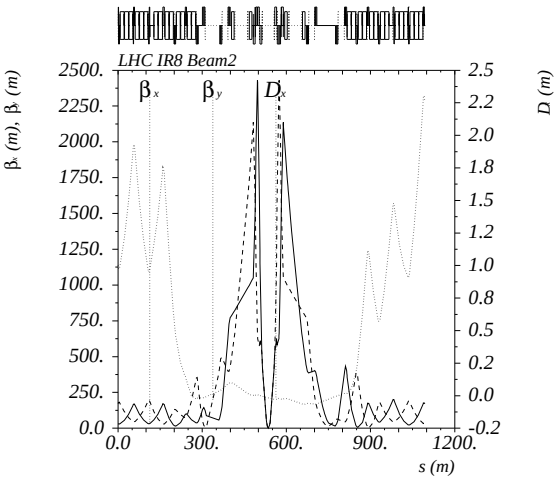

(d) Beam 2, collision optics

Figure 4.24: Injection (top) ($\beta^* = 10.0$ m) and $\beta^* = 1.0$ m collision (bottom) optics for IR8.

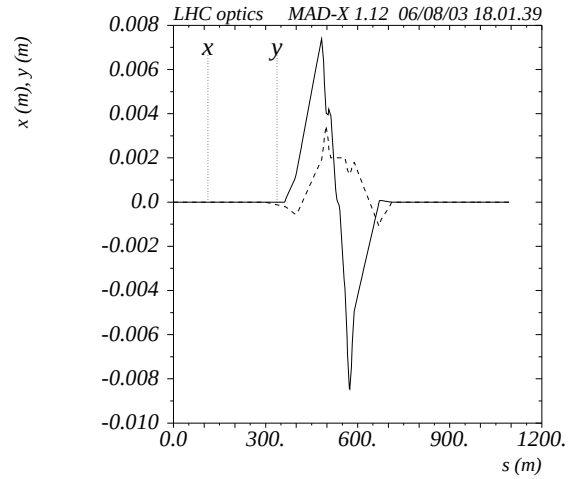

(a) Beam 1 in IR8

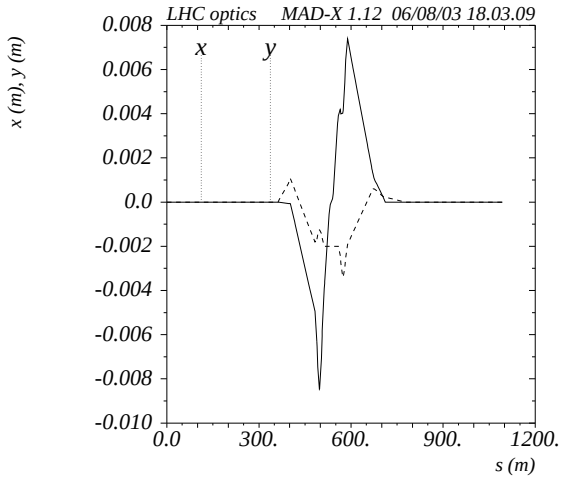

(b) Beam 2 in IR8

Figure 4.25: Crossing scheme for Beam 1 and Beam 2 at injection for the IR8.

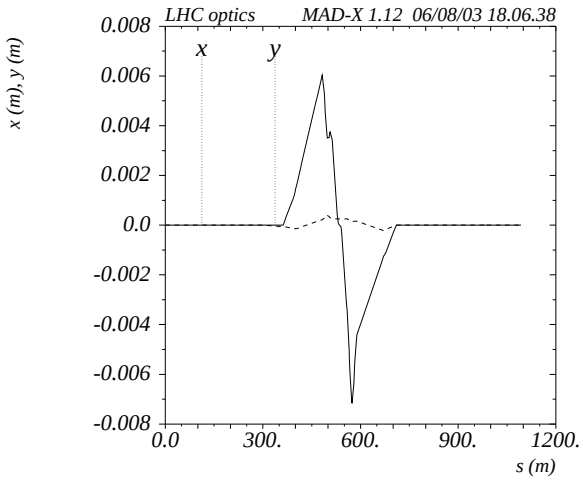

(a) Beam 1 in IR8

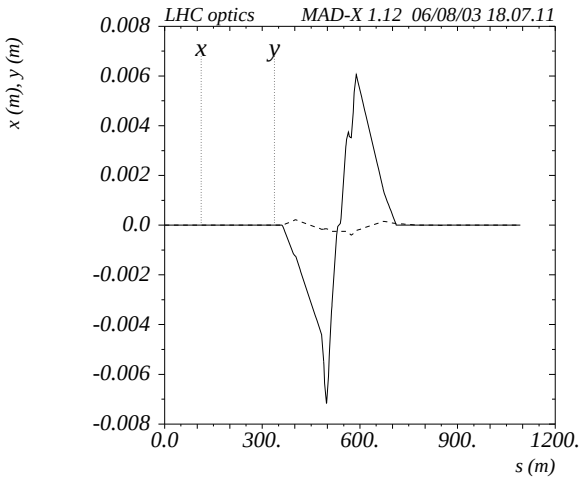

(b) Beam 2 in IR8

Figure 4.26: Crossing scheme for Beam 1 and Beam 2 at collision for the IR8 optics with $\beta^* = 1.0$ m.

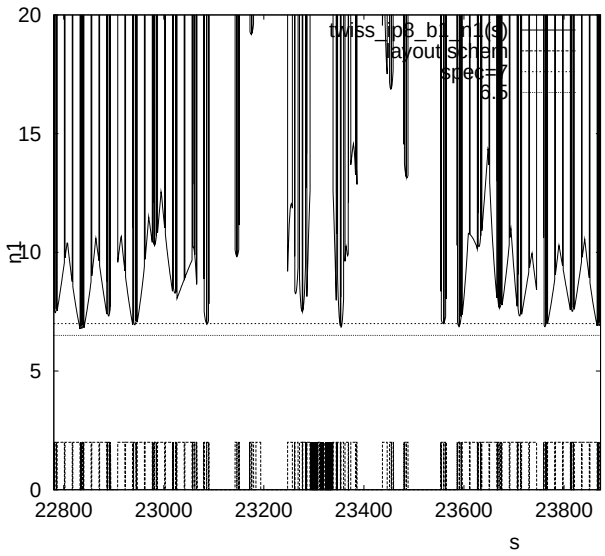

(a) Mechanical aperture of Ring 1 in IR8 at 450 GeV (injection optics)

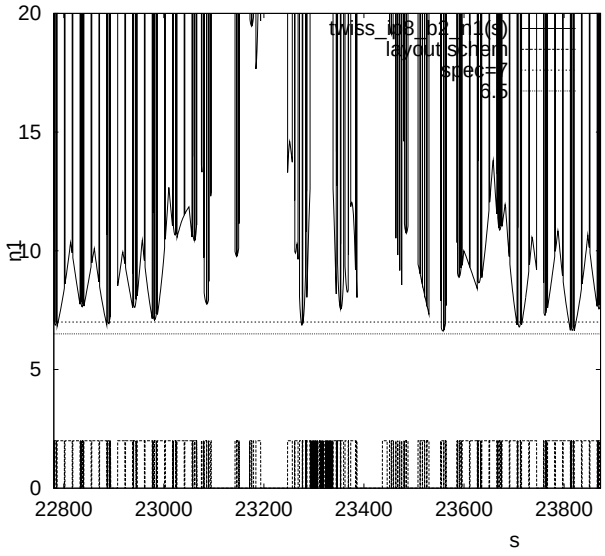

(b) Mechanical aperture of Ring 2 in IR8 at 450 GeV (injection optics)

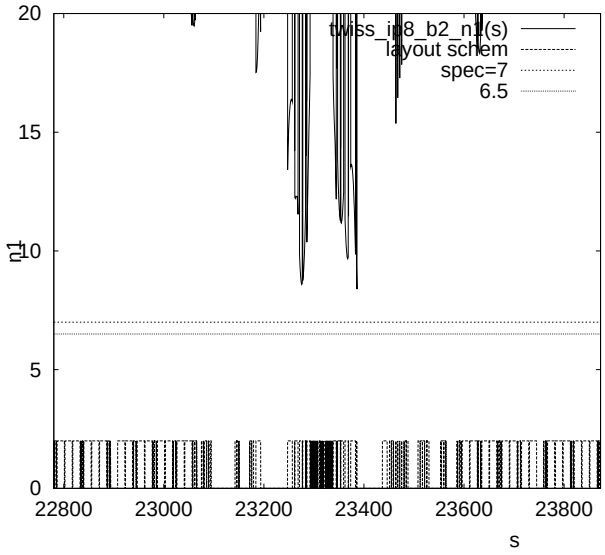

(b) Mechanical aperture of Ring 2 in IR8 at 7 TeV ($\beta^* = 1.0$ m)

Figure 4.27: The mechanical acceptance in IR8 expressed in terms of n_1 at 450 GeV (injection optics) and 7 TeV ($\beta^* = 1.0$ m). The minimum acceptance occurs for Beam 2 in Q6 and Q12 on the right-hand side of IP8.

4.3 MECHANICAL ACCEPTANCE

Expressed in beam size units, the effective aperture of the vacuum chambers of LHC are rather small, typically 10 σ. A precise two-dimensional approach is therefore used to compute the effective aperture which can be occupied by the beam. The beam shape itself deserves a particular treatment [29]. Except for a pilot beam, beam cleaning will always be in use, in particular to avoid quenches of the cryo magnets. The primary beam aperture will be delimited by the primary collimators. Secondary collimators will capture most of the secondary halo re-emitted by the primary collimators above an amplitude, which is defined as the edge of the secondary halo. The secondary beam aperture is defined by the edge of the secondary halo. The collimation efficiency will be high and thus limit the flux of the tertiary halo down to a harmless limit for the cryo magnets. It is therefore not considered in aperture calculations.

4.3.1 Beam size

All the quantities are defined in normalised coordinates:

$$X = \frac{x}{(1+k_\beta)\,\sigma_x} \quad , \quad Y = \frac{y}{(1+k_\beta)\,\sigma_y} \, , \tag{4.4}$$

with k_β being the beta-beat factor (see Tab 4.6) The primary collimators delimit the primary beam size to a regular octagon. The radius of the circle inscribed in the octagon is written:

$$X^2 + Y^2 = n_1^2 \tag{4.5}$$

with n_1 the primary collimator aperture. The secondary halo is contained in a circle of radius n_r and cut in the two principal directions at n_a (see Fig. 4.28), with:

$$n_r = 1.4 n_1 \quad , \quad n_a = 1.2 n_1 \tag{4.6}$$

These value are fixed by choosing the aperture of the secondary collimators to, see Chap 18 in this design report volume,

$$n_2 = \frac{7}{6} n_1 \tag{4.7}$$

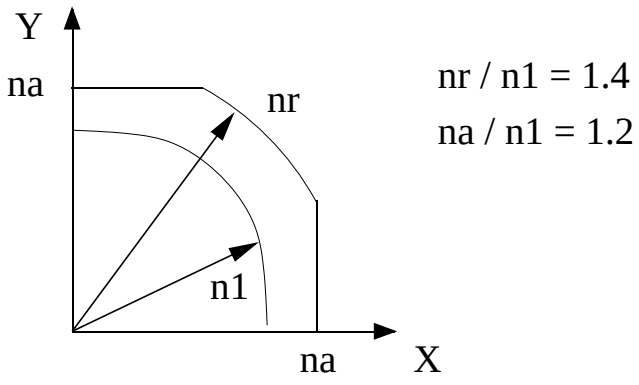

Figure 4.28: The geometry of the primary beam and its halo in normalised coordinates

At injection energy, the primary collimator aperture is specified as $n_1 = 7.0$, allowing space for the beam itself, injection oscillations and operational margins. At top energy, the same n_1 value is specified, but during the first years of operation, the secondary aperture will be $n_2 = 10$, yielding $n_r = 13.5$ (see the chapter on collimation for more details). It will be lowered down to $n_2 = 7$ after some upgrade of the cleaning system, see Tab. 4.6.

Table 4.6: Beam parameters related to aperture definitions

Variable	Name	Value	Units
Primary collimator aperture			
Injection	n_1	7	σ_β
Top energy	n_1	7	σ_β
Secondary halo			
Injection	n_r / n_a	10 / 8.4	σ_β
Top energy, early	n_r	13.5 / 11.3	σ_β
Top energy, nominal	n_r	10 / 8.4	σ_β
Radial closed orbit excursion :			
ARCs + D	CO_r^{peak}	4.0	mm
Exp.LSS at 7 TeV, Q7L to Q7R	CO_r^{peak}	3.0	mm
Beta beating	k_β	0.2	-
Relative parasitic dispersion	k_D	0.27	-
Momentum offset, injection	δ_p	1.5×10^{-3}	-
Momentum offset, collision	δ_p	0.86×10^{-3}	-

4.3.2 Beam errors

While beam dynamics is affected by random errors, the point of smallest aperture of the ring limits the performance. The aperture is therefore computed with the peak value of the errors, also called tolerance. These are listed in Tab. 4.6. Beam errors are discussed in Chap. 4.4. The maximum radial closed orbit error CO_r^{peak} is deduced from experience with LEP [30]. In collision, and in the experimental insertions, it is necessary to control the closed orbit better in order to maintain the beam in collisions. In a proton-proton collider, the superposition of the two beams is not inherently granted, contrary to e^+e^- or $\overline{p}p$ colliders. A smaller excursion is therefore used for aperture calculations.

Two sources contribute to the parasitic dispersion. A random source is dominated by orbit offsets in quadrupoles and by tilt errors of these elements. This effect is quantified by the parameter k_D given in Tab. 4.6. A substantial local effect occurs in the triplets of quadrupoles of the experimental insertions. The beams are offset by the beam-beam crossing scheme at locations where the quadrupole gradient is high and the β-functions are large. This generates a large parasitic dispersion in the other experimental insertions where the β-functions are also large. This latter contribution can be calculated by MAD and read by the code which computes the aperture. The momentum offset is made of two contributions: The aperture is computed for the particles which are at the edge of the bunch $\sigma_{\delta E/E_0}$ and the offset associated with the momentum sweep (5×10^{-4}) which will be used for chromatic measurements is added to $\sigma_{\delta E/E_0}$.

4.3.3 Mechanical tolerances

A mechanical tolerance is used for aperture calculations, instead of an rms value, for the same reason given above for beam errors. Radial tolerances are given in Tab 4.7 where the quantity t_r is the transverse radial tolerance. It applies to the centre of the vacuum chamber (cold bore in cryo-magnets), w.r.t. the survey target and including a contribution from tunnel motion for one year. They differ for different kinds of elements. Cold magnets often have larger tolerances than warm ones. The presence of a cryostat implies a further shell of structure between the vacuum chamber and the survey target. A few elements, which are located in a particular area, or which must have a small aperture for performance issues, are designed in a way that allows smaller tolerances (MQX, TCDS). The tolerance of cryo-magnets are relative to the axis of the cold bore, i.e. they represent the expected error of centering of the cold bore with respect to the central beam trajectory. An additional tolerance is added for the beam screen. The beam-screen can distort inside the cold bore. The beam-screen and cold bore tolerances are added linearly. The effective beam-screen dimensions are given in Tab 4.8. The values quoted represent the nominal mechanical dimensions, from which the tolerance of the beam screen is subtracted. This table is extracted from the Tab 2 of the Functional Specification [31].

Table 4.7: Mechanical tolerance of critical machine elements. The quantity t_r is the transverse radial tolerance. It applies to the centre of the vacuum chamber (cold bore in cryo-magnets), w.r.t. the survey target and including a contribution from tunnel motion for one year, see text.

Element	Location	t_r [mm]
Dipoles		
MB	arc	2.0
MBX, MBRC	exp. IR	1.6
MBXW	IR1,IR5	1.0
MBW	IR3,IR7	1.6
MBRS, MBRB	IR4	2.0
Quadrupoles		
MQ, MQM	arc, IR's	1.5
MQX	exp. IR	1.2
MQW	IR3,IR7	1.6
Absorbers		
TAS	IR1,IR5	1.0
TAN	IR1,IR5	2.6
TCDS	IR6 absorbers	0.5
Kicker and Septa		
MKI	inj. kicker	1.0
MKD	dump kicker	2.0
MSI	inj. septum	2.0
MSD	dump septum	1.0
ADT	RF dampers	1.5

Table 4.8: Beam screen type with the corresponding cold bore inner/outer diameters, the effective inner diameter of the beam screen and the effective full inner width of the flat segments of the beam screen.

Beam screen type	Colb bore ID/OD [mm]	$d_{\rm bs}$ [mm]	$h, v_{\rm bs}$ [mm]
50A	50/53	44.0	34.3
50L	50/53	45.2	35.4
53	53/57	47.8	38.0
63	63/66.5	57.9	48.1
69	69.1/73	62.7	52.9
74	74/78	67.5	57.7

4.3.4 Effective aperture

The effective normalised aperture is calculated for each element at location s separated by ≈ 1 m. The beam centroid is shifted by the sum of all the transverse displacements of either the beam itself or the cold bore:

$$\vec{\Delta}(s) = \vec{d}_{\rm sep}(s) + \vec{d}_{\rm axis}(s) + \vec{d}_{\rm inj}(s)\,, \tag{4.8}$$

with $\vec{d}_{\rm sep}(s)$ the orbit generated by the beam-beam crossing scheme, $\vec{d}_{\rm axis}(s)$ the transverse displacement of separation and dog-leg dipoles with respect to the central trajectory, $\vec{d}_{\rm inj}(s)$ the beam displacement of the injected beam up to the injection kicker, and up to the TDI absorber in case of kicker misfire. The mechanical tolerance and the closed orbit displacement are defined radially. The corresponding offset is:

$$\vec{u} = (t_r + CO)(\cos\alpha, \sin\alpha) \quad \text{with} \quad \alpha\,\epsilon\,[\,0\,,\,\pi/2\,]\,, \tag{4.9}$$

Table 4.9: Cold bore size and beam screen and orientation in cryo-magnets. The first column indicates the temperature of the helium bath. The second one contains the cold inner and outer diameters and the corresponding beam screen type (in boldface). The orientation of the beam screen is given for each insertion and each element in the remaining columns. The beam-screen dimensions are given in Tab. 4.8.

C. B. T [K]	ID/OD [mm] **BS**	ir1	ir2	ir3	ir4	ir5	ir6	ir7	ir8
4.5	50/53 **50A**	Q6L VH Q5L HV Q5R VH Q6R HV	Q6L HV Q5R HV Q6R VH	Q6L VH Q6R HV		Q6L VH Q5L HV Q5R VH Q6R HV		Q6L VH Q6R HV	Q6L HV Q5L VH Q6R VH
1.9	50/53 **50L**	Q7 VV SM	Q7 VV SM	Q7 VV SM	Q7 VV SM	Q7 VV SM	SM	Q7 VV SM	Q7 VV SM
1.9	53/57 **53**	Q1 H	Q1 H			Q1 V			Q1 V
4.5	63/66.7 **63**	Q4 VV	Q5L HH Q4 HH		Q6L HV Q5L VH Q5R HV Q6R VH	Q4 VV	Q5L VH Q4L HV Q4R VH Q5R HV		Q5R HH Q4 HH
1.9	63/66.7 **63**	Q2 H Q3 H	Q2 H Q3 H			Q2 V Q3 V			Q2 V Q3 V
4.5	69.1/73 **69**	D2 VV	D2 HH		D4L VH D3L VH D3R VH D4R HV	D2 VV			D2 HH
1.9	74/78 **74**	DFBX	D1 V DFBX			DFBX			D1 V DFBX

see Tab. 4.7 for t_r and Tab. 4.6 for CO. The calculation is made for several values of α (default is 5). Finally the contribution of parametric dispersion is:

$$\vec{d}_{\rm disp}(s) = (1+k_\beta)\left[\vec{D} + k_D \frac{D_{\rm x,QF}}{\sqrt{\beta_{\rm x,QF}}}\sqrt{\vec{\beta}}\right]\,\delta_p, \tag{4.10}$$

with δ_p the relative momentum offset, see Tab 4.6. The total offset is then

$$\overrightarrow{OO'}\,(s) = \vec{\Delta}(s) + \vec{u} + \vec{d}_{\rm disp}(s)\,. \tag{4.11}$$

Finally the aperture is calculated by first stretching the secondary halo, defined in Fig 4.28 and Tab 4.6, with the factor $(1+k_\beta)\,\sigma_x$ and $(1+k_\beta)\,\sigma_y$ along the X and Y directions respectively. Then it is shifted with $\overrightarrow{OO'}\,(s)$. Its size is adjusted to the largest value which is still inscribed in the beam screen or the vacuum chamber as shown in Fig 4.29. The normalised primary aperture is the corresponding value $n_1(s)$ which is the maximum acceptible primary collimator opening that still provides a protection of the mechanical aperture against losses from the secondary beam halo. An aperture plot for a section of the ring is produced, which displays the function $n_1(s)$. The aperture of this section is the minimum value of the function $n_1(s)$. The orientation of the beam screens inside the insertion regions is optimized for a maximum mechanical aperture and Tab. 4.9 lists the beam screen orientation for the insertion region elements. All beam screens have a race track shape and 'H' and 'V' indicate that the flat part of the beam screen lies in the horizontal or vertical plane.

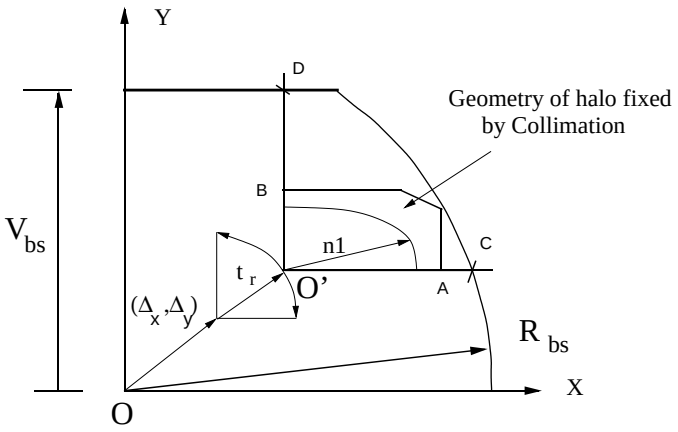

Figure 4.29: The largest secondary halo which fits to the inner edge of the beam screen, once shifted by the sum of the factors discussed in the text.

4.4 BEAM AND MACHINE PARAMETER TOLERANCES FOR OPERATION

The specification of the LHC beam and machine parameter tolerances for operation is based on simulation studies and past operational experience from existing hadron storage rings. Tab 4.10 summarizes the main optics tolerances and Tab 4.11 the main beam tolerances.

Table 4.10: *Operational optics tolerances.*

Parameter	tune	coupling	chromaticity	orbit (global)	orbit (local)	β-beat	dispersion spurious / normalized
Limit	$\pm 3 \times 10^{-3}$	$\lvert c_- \rvert \ll 3^{-3}$	± 2.0	4 mm	$0.1\ \sigma$	20 %	27 %

Table 4.11: *Operational tolerances for the main beam parameters.*

Parameter	N_{bunch}	$\epsilon_{\mathrm{trans}}$	orbit (IP)	X-ing (IP)
Limit	10%	20%	10% of RMS beam size	10% of x-ing angle

4.4.1 Fractional tunes

Resonances of the horizontal and vertical particle oscillations limit the single particle stability and the control of the fractional tunes is of great importance for the preservation of the dynamic aperture. The choice for the fractional part of the base line LHC working point at injection ($Q_x = 59.28$ and $Q_y = 64.31$) is based on operational experience and various tracking studies. For example, Fig. 4.32 shows the 1000 turn dynamic aperture (DA) for the Version 5.0 lattice of the LHC and indicates that the injection tunes of the LHC lie at the centre of a plateau with sufficiently large DA [32]. The width of this plateau is approximately $\Delta Q \approx 10^{-2}$. Combining the width of this plateau with the total expected detuning from the field imperfections yields an operational margin of $\Delta Q_{\mathrm{inj}}(\mathrm{operation}) \approx \pm 3 \times 10^{-3}$ [33].

The choice for the fractional part of the tune at collision ($Q_x = 59.31$ and $Q_y = 64.32$) is based on the operational experience from the $Sp\bar{p}S$ collider [34]. The operational margin for the tunes during collisions is determined by the total tune spread due to the beam-beam interactions and field imperfections yielding an operational tolerance of $\Delta Q_{\mathrm{col}}(\mathrm{operation}) \approx \pm 2.5 \times 10^{-3}$ for the nominal beam parameters. This margin disappears for the operation with ultimate beam parameters.

4.4.2 Coupling

A proper tune control requires a machine coupling which is smaller than the tune separation in the horizontal and vertical planes. In the presence of coupling the minimum tune separation in the machine can be written as:

$$|Q_I - Q_{II}| = \sqrt{(Q_x - Q_y - p)^2 + |c_-|^2}, \tag{4.12}$$

where c_- is the coupling coefficient. For the LHC this requirement yields an operational tolerance for the global machine coupling of $|c_-| \ll 0.03$ and $|c_-| \ll 0.01$ for the injection and collision optics respectively.

4.4.3 Orbit

The maximum acceptable closed orbit perturbations are limited by the mechanical aperture and the feed-down effect of non-linear field imperfections. Both requirements limit the peak orbit perturbations to $|\Delta CO| \leq 4$ mm. This orbit tolerance is compatible with experience from the LEP operation [30]. Tighter orbit tolerances apply for special areas in the LHC (e.g. the collimation insertions and the beam dump area). These local tolerances require peak orbit deviations of $|\Delta CO(local)| \leq 0.1\ \sigma$ and are discussed in Chaps. 17 and 18.

4.4.4 $\beta - beat$

The maximum acceptable β-beat is limited by the available mechanical aperture and non-linear particle motions due to the magnet field imperfections. For the LHC the total tolerance for the β-beat has been specified as $20\ \%$.

4.4.5 Chromaticity

The operational margins for the chromaticity are based on collective instabilities and the operational experience in existing hadron storage rings [34]. Stability of collective effects requires positive chromaticity values and operational experience chromaticity values smaller than 5 units yielding a target chromaticity of 2 units with an operational margin of $\delta Q^{'} = \pm 2$.

4.4.6 Spool piece powering

In order to maximize the DA, the LHC features spool piece correction circuits which aim at an arc-by-arc correction of the b_3, b_4 and b_5 field errors of the main dipole magnets. The DA reduction due to an imperfect spool piece circuit powering has been studied in [35] and [36]. Taking a DA reduction of more than $0.5\ \sigma$ as a measure for the maximum tolerance of the spool piece circuit powering one obtains a minimum correction accuracy of 50 % for the powering of the b_3 circuits (assuming that the total chromaticity is corrected via the lattice sextupole circuits), 30 % for the octupole circuits (b_4) and 80 % for the b_5 circuits, where 100 % represents a perfect powering of the spool piece circuits and 0 % no powering at all.

4.5 FIELD QUALITY SPECIFICATION

4.5.1 Introduction

The magnetic field expansion used for the LHC magnets reads [37]:

$$B_y + iB_x = B_{ref} \sum_{n=1}^{\infty} (b_n + ia_n) \left(\frac{x + iy}{R_r} \right)^{n-1} \tag{4.13}$$

The subscript $n = 1$ refers to a dipole, $n = 2$ to a quadrupole and so on. The terms a_n and b_n indicate skew and normal harmonics respectively and $B_{\rm ref}$ represents the magnetic field at the reference radius $R_r = 17$ mm. The multipolar harmonics, a_n and b_n can be classified as:

- those inherent to the *design geometry* (including the contribution of the beam-screen) are called 'systematic'.

They respect the coil symmetry (as b_1, b_3, b_5, ... for a dipole magnet and b_2, b_6, b_{10} for a quadrupole) or, at least, the symmetry given by the horizontal mid-plane (as the harmonics b_2 or b_4 which, due to the two-in-one design of the main dipoles, have opposite sign in the inner and outer bores of the magnet).

- those due to *fabrication tolerances* of the different components and of the tooling used during assembly. They are called 'uncertainty' errors in the following.

In principle, these errors do not respect any symmetry and are responsible for any skew harmonics such as the significant a_2 harmonics expected in the main dipole magnets. They are most likely random and/or lead to an average deviation with respect to the systematic components inherent to the magnet design. In this case, the 'uncertainty' will vary from production line to production line in the case of the short series of magnets (e.g. matching section quadrupoles MQMC, MQM or MQML, triplet quadrupoles or warm magnets). On the other hand, concerning the main dipole and quadrupole magnets, the concept of uncertainty must be interpreted as an average deviation per arc with respect to the systematic, changing from arc to arc and reflecting possible trends and/or modification of cross-section during the production and the fact that, for the main dipoles, the percentage of the magnets coming from three manufacturers might not be kept constant in each of the eight sectors of the machine.

- those generated by the *persistent currents* in the superconducting cables.

They are responsible for systematic errors for the allowed harmonics (e.g. b_1, b_3, b_5, ... for a dipole magnet), possibly changing from arc to arc depending on the cable manufacturer equipping a given sector (i.e. source of uncertainty for the main dipoles and the main quadrupoles), but also for random errors for all other harmonics, a_n and b_n.

- those due to inter-strand *eddy currents* during the ramp, or ramp induced errors proportional to dI/dt.

They are inversely proportional to the inter-strand contact resistance R_c. The latter being presently much larger than targeted, the ramp induced errors measured in the first main dipole magnets have been found small enough to be neglected during the operation of the LHC and, therefore, will not be discussed in the following.

- finally, those induced at high field by *saturation*.

The first two sources of error, of purely geometric origin, are present at each stage of the LHC cycle (injection, ramp, collision), while the persistent current induced errors are maximum at the injection energy, these perturbations die away when raising the current (following a power law in $1/B^{1.5}$) and significant saturation effects can take place at nominal field, affecting in particular the sextupole component of the main dipoles.
To summarize, the multipolar content of each magnet installed in the ring is presently modelled as:

$$b_n = b_{n_S} + \frac{\xi_U}{1.5} b_{n_U} + \xi_R b_{n_R} \,, \tag{4.14}$$

where ξ_U and ξ_R denote random numbers with a Gaussian distribution cut at 1.5 and 3σ, respectively. Following the above discussion, b_{n_S} refers to a systematic error, b_{n_U} represents a maximum possible deviation with respect to the systematic, changing from sector to sector for the MB's or MQ's or from production line to production line for the other type of magnets produced in short series, and b_{n_r} denotes the standard deviation of the random errors varying from magnet to magnet. It is clear that each of these three quantities depends on the type of magnet considered but also on the operation mode of the LHC, that is, for instance, by summing the errors of geometric origin either with the persistent current induced errors at injection or with the saturation effects at high field.
Finally it is worth noting that the present modeling of the machine assumes that the uncertainty corresponds to

1.5 σ of a normal distribution cut at 1.5 σ. With this definition, the standard deviation related to the concept of uncertainty is then given by:

$$\begin{aligned} \sigma\left[b_{n_U}\right] &= \left\{\frac{1}{\sqrt{2\pi}}\int_{-1.5}^{1.5} dx\, x^2\, e^{-x^2/2}\right\}^{1/2} \frac{b_{n_U}}{1.5} \\ &= 0.69\,\frac{b_{n_U}}{1.5} = 0.46\; b_{n_U}\,. \end{aligned} \tag{4.15}$$

Since for the main dipole and quadrupole magnets, the uncertainty errors are assumed to be uncorrelated from arc to arc, with a confidence level of more than 99%, the bias induced is given by:

$$\langle b_{n_U}\rangle = \pm\frac{3}{\sqrt{8}}\,\sigma\left[b_{n_U}\right] = \pm\,0.49 b_{n_U}\,. \tag{4.16}$$

This relation will be of major interest, in particular to correctly interpret the specification concerning the uncertainty of b_2 and b_4 of the main dipole magnets. Indeed, due to the symmetry of the 2-in-1 design of the LHC dipole magnets both the systematic b_2 and b_4 errors have opposite signs in the inner and outer bores of the magnets. Because the particles of either beam travel an equal distance in the inner and outer apertures of the ring, these systematic errors inherent to the magnet design have no impact on the global beam observables such as the tune or the amplitude detuning, which is not the case for the uncertainty of b_2 and b_4.

4.5.2 Summary of the main dipole target field errors specifications

Concerning the injection optics, since the main dipoles occupy 66 % of the circumference of the LHC ring, they are the most demanding in terms of field quality while, in collision, the high β-function in the squeezed insertions makes the triplets and the separation-recombination dipoles D1/D2 the most critical magnets of the LHC ring (see Sec. 4.5.4). The performance of the main dipoles in terms of field quality have been analysed in detail in [33]. Starting from the expected field error table 9901 elaborated in 1999 by the Field Quality Working Group (see also [33, pp.65–67]) and based on criteria of a different nature such as the control of mechanical and dynamic aperture at injection and/or the correctability of the closed orbit, coupling and linear chromaticity up to 7 TeV. Hard limits have be found for the most critical multipoles and are reported in Tab 4.12. (More information on the field quality specification based on the DA evaluations can be found in Sec 4.7.3).
These specifications strongly depend on the misalignments of the different LHC components. The most sensitive ones are listed below.

- The tolerances on the multipoles a_1 and b_1 are directly linked to the positioning errors of the main quadrupole magnets in the LHC tunnel. According to [38], the quadrupole misalignments should not exceed 0.36 mm (rms) including the survey errors at installation and the effects induced by the ground motion after one year.

- The tolerance for the systematic b_3 component at injection is only based on the quadrupolar feed-down effects induced by the random misalignments of the MCS spool-piece with respect to the dipole. The latter have be specified to be lower than 0.5 mm (rms).

- The specification of the uncertainty of a_4 might be further tightened in case of systematic vertical misalignment of the b_5 spool-piece, MCD, of more than 0.3 mm.

Any deviation from these values could significantly relax or tighten the tolerances given for the field quality of the main dipoles. Inversely, if the field imperfections of the main dipoles significantly improve during the production, the above alignment tolerances could also be relaxed.
Finally, it is worth noting that the specification of 3 units for the systematic b_3 both at the end of the ramp (i.e close to 7 TeV with a maximum ramp rate of 10 A/s) and in collision, leaves a margin of 1.35 units for the MCS corrector strength at high field (see Tab. 3.1). In case of a failure of the MCS circuits in one or two sectors of the machine (for instance caused by repetitive quenches at high current of one single spool-piece per MCS circuit), this margin will just be sufficient to pursue the run of the LHC without requesting an intervention of 2 or 3 weeks to disconnect the pathological magnet.

Table 4.12: Specifications for the field quality of the main dipole magnets at injection, end of ramp and in collision (a_n and b_n given in units of 10^{-4} relative field error at a reference radius $R_{\rm ref} = 17$ mm).

Harmonics a_n & b_n	Injection optics (450 GeV)	Injection optics (end of ramp)	Collision optics (7 TeV)	Systematic (max. value)	Uncertainty (max. value)	Random (r.m.s)	Criteria used
b_1	×	×	×	None	6.5	8.0	Closed orbit at injection and MCB strength at 7 TeV (with the MQ's misaligned by 0.36 mm r.m.s.)
a_1 (including MB roll angle)	×	×	×	6.5 (averaged per arc cell)		8.0	
b_2	×		×	1.4	0.8	0.7 0.8	β-beating and IP phasing
a_2	×	×	×		0.9	1.9 2.3 1.6	Vertical dispersion, linear coupling and MQS strength at 7 TeV
b_3	×		×	10.7 (including the 3.0 bias due to 3.0 uncertainty)		1.4 none 1.8	b_2 feed-down (with the MCS's misaligned by 0.5 mm r.m.s. w.r.t. the MB's) and DA at injection Correction of Q' and MCS strength at 7 TeV
a_3	×		×		1.5	0.7	Chromatic coupling inducing Q'' and MSS strength at 7 TeV
b_4	×		×	± 0.2 (from Table 9901)	0.4	0.5	DA and Q'' at injection, Detuning $\partial Q/\partial J$ and MCO strength at 7 TeV
a_4	×				0.13	0.5 (from Table 9901)	DA at injection (considering the MCD's systematically) misaligned by 0.3 mm w.r.t. the MB's)
b_5	×		×	1.1 (including the 0.8 bias due to uncertainty)		0.5 0.4	DA and Q''' at injection, Detuning $\partial^2 Q/\partial J \partial \delta$ and MCD strength at 7 TeV
a_5	×				0.4	0.4 (from Table 9901)	Off-momentum DA at injection
b_7	×			$-0.3 < \langle b_7 \rangle < 0.1$		0.2 (from Table 9901)	DA at injection
a_6, b_6, a_7 and higher order multipoles	×			OK with the Error Table 9901			DA at injection

4.5.3 Main quadrupole and Short Straight Section assembly

The field quality of the elements of the short straight section (MQ, MQT, MS(S), MCB(H,V), MO) should be such that the effect on the relevant parameters is in the shadow of the effect of the main bending magnets. In this report the general procedure and the final results are reported, whereas details can be found in [33] and [39]. Two types of errors were considered: the field harmonic errors and the alignment errors. The cases considered are summarized in the following subsections.

Random b_2 errors in the MQ magnets

The effect of a random b_2 in the MQ has been analyzed numerically with the help of MAD [40]. A random b_2 error in the MQ magnets generates beta and dispersion beating. Mechanical aperture considerations [33] set the limits to 15% for the beta beating and 3.9 10^{-2} $m^{-1/2}$ for the normalized dispersion. Calculations with MAD for a random b_2 error of 10 units (target value in Tab 4.13 and 4.14) yield a maximum effect of 12 % for the beta beating and 2.6 10^{-2} $m^{-1/2}$ for the dispersion beating. Both values are within the tolerances.

Random b_3 errors in MQ magnets

The first order effect of a b_3 component in the MQ is the change of the chromaticity of the machine. This error can be compensated by the adjacent sextupoles MS. It has been verified that an error several times bigger than reported in the error Tab 4.13 and 4.14 can be correct with the sextupoles. The maximum allowed b_3 will be limited by DA considerations.

Multipoles higher than b_2 in the MQ magnets

The effect of the MQ higher order multipoles should not impact the reference dynamic aperture of 11.5 σ. This value is obtained by observing the behaviour of particles over 10^5 turns for 60 different MB error configurations as explained in 4.7 . The minimum DA for a machine without MQ errors and one with MQ errors has been compared : the MQ errors in Tab 4.13 and 4.14 do not significantly impact the dynamic aperture. However, tracking studies with slightly increased b_6 multipole errors showed a reduction of the DA indicating that the b_6 given in Tab 4.13 and 4.14 is at the limit of the acceptable field imperfections. Tab 4.13 and 4.14 summarize the MQ field errors which are referenced as error Table 0210.

Table 4.13: Normal Multipoles for MQ-table 0210. Columns 'p', 'g' and 'r' specify the persistent current, geometric and ramp induced errors respectively.

	mean			uncertainty			random		
n	p	g	r	p	g	r	p	g	r
1	0	0.483	0	0	0	0	0.747	0	0.941
2	-5.6	0	16.82	0.56	10	5.01	0.5	10	2.7
3	0	0.007	0	0	0.51	0	0.362	0.85	1.7
4	0	0.514	0.202	0	0.578	0	0	0.289	0.578
5	0	-0.005	0	0	0.246	0	0.133	0.231	0.246
6	-4.51	3.599	0.167	0.451	0.251	0.049	0.058	0.418	0.1
7	0	0	0	0	0	0	0	0.142	0
8	0	0.217	0	0	0	0	0	0.241	0
9	0	0	0	0	0	0	0	0.41	0
10	0.126	-0.418	-0.056	0.014	0.698	0.021	0	0.349	0
11	0	0	0	0	0	0	0	0.237	0

Tolerances on alignment

Tolerances from [38] are summarized in Tab 4.15

Table 4.14: Skew Multipoles for MQ-table 0210

	mean			uncertainty			random		
n	p	g	r	p	g	r	p	g	r
1	0	0	0	0	0	0	0.747	0	0.941
2	0	0	0	0	0	0	0	0	0.5
3	0	0	0	0	0.51	0	0.362	0.85	1.7
4	0	0	0	0	0.578	0	0.384	0.289	1.156
5	0	0	0	0	0.246	0	0.133	0.187	0.246
6	0	0	0	0	0.251	0	0	0.418	0.1
7	0	0	0	0	0	0	0	0.142	0
8	0	0	0	0	0	0	0	0.241	0
9	0	0	0	0	0	0	0	0.41	0
10	0	0	0	0	0	0	0	0.349	0
11	0	0	0	0	0	0	0	0.237	0

Table 4.15: Random and systematic alignment tolerances for the elements of the SSS

element	position x mm	position y mm	roll mrad
MQ	0.37	0.37	1.0 (r) / 0.3(s)
MS	1 (r) 0.1(s)	0.8 (r) 0.1(s)	1.5(r) 2.0(s)
MO	1.9 (r) / 0.16(s)	0.5 (r) / 0.1(s)	1.5(r) / 1.0(s)
CO			0.6

Higher order mutipoles in MQT,MS(S), MCB and MO

It has been verified that the multipoles generated by an error in coil positioning of 0.1 mm can be tolerated in the orbit correctors and in the sextupoles [39]. The maximum tolerable high order multipoles can be determined by rescaling from the MQ or the MB case with the following considerations:

- each MQ in the SSS is equipped with an MS or MSS. The MS(S) should not contribute to each multipole by more than 1% . Rescaling - over the integrated field at the reference radius - with respect to the target value in Tab 4.13 and 4.14 brings the value of Tab 4.16. The procedure is equivalent for MQT and MO.

- MCBH/V : due to the function of this corrector the rescaling is done with respect to the main bending magnets.

4.5.4 Insertion magnets

The approach used is not too different from the one applied for the main dipoles. Tolerances on the alignment of the insertion quadrupoles are given by considering the influence on closed orbit correctability (transverse misalignments and longitudinal tilt), coupling compensation and magnitude of spurious vertical dispersion (transverse tilt), beta-beating (longitudinal alignment). As far as the field errors are concerned, target intervals for the linear components (b_2, a_2) are found by imposing a bound on the beta-beating generated, while the ultimate criterium for determining the tolerances of the nonlinear field components is the outcome of detailed tracking studies. Normally, the field errors of the elements under study are compared to similar magnets for which tracking results are already known, taking into account the proper scaling given by the beta-functions. This is, for example, the case of the MQM, MQML, MQMC quadrupoles which are compared to the main quadrupoles requiring their contribution (to first order) be in the shadow of the main quadrupoles. Using these values as input for tracking allows the computations to be faster [41].

Table 4.16: Target field error tolerances for MQT, MS, MCB and MO units of the SSS assembly.

random	b1	b2	b3	b4	b5	b6	b7	b8	b9	b10	b11
MQT+MQS	1.34	18.02	1.66	0.52	0.481	0.76	0.26	0.43	0.74	063	0.43
MS+MSS	1.86	24.9	2.3	0.719	0.664	1.05	0.35	0.6	1.02	0.868	0.590
MO	9.59	128.6	12	3.817	3.576	5.73	1.96	3.37	5.81	5.02	3.41
MCBH/V	37.6	3.293	8.38	0.34	0.974	0.06	0.26	0.02	0.07	0.01	0.01
systematic	b1	b2	b3	b4	b5	b6	b7	b8	b9	b10	B11
MQT+MQS	0.869	-1.06	0.47	1.445	0.23	-1.18	0	0.39	0	0.103	0
MS+MSS	1.2	-1.47	0.65	1.997	0.318	-1.62	0	0.54	0	0.142	0
MO	6.2	-7.60	3.41	10.61	1.714	-8.87	0	3.03	0	0.819	0
MCBH/V	0	5.598	-14	0.052	2.766	-0.03	0.36	0.01	0.46	0	0.264
random	a1	a2	a3	a4	a5	a6	a7	a8	a9	a10	a11
MQT+MQS	1.34	0.00	1.66	0.87	0.41	0.75	0.26	0.43	0.74	6.28	4.27
MS+MSS	1.86	0.00	2.30	1.20	0.57	1.04	0.35	0.60	1.02	8.68	5.90
MO	9.59	0.00	12.03	6.35	3.07	5.68	1.96	3.37	5.81	50.16	34.06
MCBH/V	1.88	8.77	1.68	1.34	0.66	0.24	0.08	0.07	0.07	0.01	0.00
systematic	a1	a2	a3	a4	a5	a6	a7	a8	a9	a10	a11
MQT+MQS	0.00	0.00	0.46	0.52	0.22	0.22	0.00	0.00	0.00	0.00	0.00
MS+MSS	0.00	0.00	0.63	0.72	0.31	0.31	0.00	0.00	0.00	0.00	0.00
MO	0.00	0.00	3.32	3.82	1.65	1.70	0.00	0.00	0.00	0.00	0.00
MCBH/V	44.18	3.44	5.22	0.49	1.57	0.12	0.05	0.00	0.10	0.00	0.03

The detailed results of these studies can be found in [41, 42, 43, 44]. A qualitative summary of the main conclusions is reported here:

- MQM, MQMC, MQML [41]: these magnets are very similar to MQs not only as far as the mechanical structure is concerned, but also for the values of the optical functions. In the following we assumed the same field quality errors as for the MQ's (see Tabs. 4.13 and 4.14).

- MQY [41]: they are large bore quadrupoles, hence structurally different from MQs, and are located in regions where the beta-functions assume values larger than those in the arc-cell, both for the injection and collision optics. This implies that, at injection, the target values for the field quality are necessarily tighter than those of the MQs. At high-energy they should be compared, as far as the field errors are concerned, with the triplet quadrupoles with possibly some relaxed constraints due to the smaller beta-function than the triplet assembly.

- MQW [42, 43]: these warm quadrupoles are planned to be installed in the insertions 3 and 7. Saturation effects make the distance between the magnetic centre of the two quadrupole bores different from the nominal beam transverse separation, thus generating a dipole kick, inducing a closed orbit distortion. In addition, the dependence of saturation on beam energy induces a dynamic closed orbit distortion which however, seems not to be critical for the LHC operation and in particular, for the performance of the collimation system [42]. As far as higher order effects are concerned, the measured field errors [45] have been used in tracking studies and found to be compatible with the target value of dynamic aperture [43].

- D1/D2 [44]: the cold separation/recombination magnets have been studied in detail and their influence for the dynamic aperture evaluated using the expected error tables [46] to generate the nonlinear field errors. Also in this case, the error tables turned out to be compatible with the requirements on the value of the dynamic aperture.

Table 4.17: Multipole errors of the D1 magnet (main body).

	Normal multipoles						Skew multipoles					
n	Mean		Uncertainty		Random		Mean		Uncertainty		Random	
	p	g	p	g	p	g	p	g	p	g	p	g
1	0.0000	0.0000	0.0000	0.0000	0.0000	0.0000	0.0000	0.0000	0.0000	0.0000	0.0000	0.0000
2	-0.1088	0.1904	0.0000	0.5440	0.0000	0.1904	-0.2720	0.4080	1.5230	2.3596	0.1199	1.0540
3	-4.1431	-2.1825	1.9465	1.5860	0.3606	0.8416	0.1064	-0.1387	0.0000	0.2682	0.0000	0.0971
4	-0.0377	0.0220	0.0000	0.0786	0.0000	0.0283	0.0377	0.0063	0.1495	0.3396	0.0000	0.1321
5	0.0748	0.0599	0.0551	0.1732	0.0195	0.0877	0.0043	-0.0150	0.0000	0.0406	0.0000	0.0128
6	0.0189	-0.0189	0.0000	0.0174	0.0000	0.0058	0.0029	-0.0073	0.0000	0.0814	0.0000	0.0247
7	-0.1443	0.1058	0.0091	0.0198	0.0000	0.0109	0.0010	-0.0010	0.0000	0.0069	0.0000	0.0030
8	-0.0013	-0.0007	0.0000	0.0027	0.0000	0.0007	0.0000	-0.0007	0.0000	0.0101	0.0000	0.0034
9	0.0064	0.0014	0.0023	0.0055	0.0000	0.0023	0.0009	-0.0009	0.0000	0.0014	0.0000	0.0005
10	-0.0003	0.0016	0.0000	0.0019	0.0000	0.0006	-0.0006	0.0012	0.0009	0.0012	0.0000	0.0006
11	-0.0013	-0.0123	0.0006	0.0008	0.0000	0.0004	0.0000	-0.0002	0.0000	0.0004	0.0000	0.0002

Table 4.18: Multipole errors of the D1 magnet (lead end).

	Normal multipoles						Skew multipoles					
n	Mean		Uncertainty		Random		Mean		Uncertainty		Random	
	p	g	p	g	p	g	p	g	p	g	p	g
1	0.0000	0.0000	0.0000	0.0000	0.0000	0.0000	0.0000	0.0000	0.0000	0.0000	0.0000	0.0000
2	0.0952	-0.3196	0.0000	1.5368	0.0000	0.6732	-0.6596	-0.9656	0.0000	2.9036	0.0000	1.2036
3	-1.5953	10.3346	0.0000	1.3548	0.0000	0.5086	-0.0370	-4.5546	0.0000	0.4670	0.0000	0.1803
4	0.0031	0.0126	0.0000	0.2295	0.0000	0.0723	-0.0660	0.0283	0.0386	0.2358	0.0000	0.0912
5	0.0363	-0.0919	0.0252	0.1475	0.0000	0.0470	0.0064	0.4768	0.0167	0.0641	0.0000	0.0278
6	-0.0029	0.0029	0.0000	0.0422	0.0000	0.0174	-0.0044	0.0015	0.0159	0.0422	0.0000	0.0145
7	0.0138	0.0910	0.0000	0.0109	0.0000	0.0049	0.0030	-0.0850	0.0000	0.0129	0.0000	0.0059
8	0.0000	0.0000	0.0000	0.0040	0.0000	0.0020	0.0007	-0.0013	0.0000	0.0054	0.0000	0.0020
9	-0.0009	-0.0018	0.0000	0.0037	0.0000	0.0014	-0.0005	0.0114	0.0000	0.0023	0.0000	0.0009
10	0.0000	-0.0003	0.0000	0.0025	0.0000	0.0009	0.0000	-0.0003	0.0009	0.0012	0.0000	0.000
11	0.0000	-0.0013	0.0000	0.0006	0.0000	0.0002	0.0000	-0.0008	0.0005	0.0004	0.0000	0.0002

Table 4.19: Multipole errors of the D1 magnet (return end).

	Normal multipoles						Skew multipoles					
n	Mean		Uncertainty		Random		Mean		Uncertainty		Random	
	p	g	p	g	p	g	p	g	p	g	p	g
1	0.0000	0.0000	0.0000	0.0000	0.0000	0.0000	0.0000	0.0000	0.0000	0.0000	0.0000	0.0000
2	0.0136	0.1496	0.4555	1.2308	0.0000	0.4488	-0.8500	0.6188	0.5796	3.0600	0.0000	1.2988
3	-0.9849	2.8114	0.0000	1.2346	0.0000	0.5364	-0.0139	0.1341	0.0665	0.4763	0.0000	0.1572
4	0.0031	0.0000	0.0000	0.1132	0.0000	0.0503	-0.0755	0.0755	0.0000	0.2295	0.0000	0.0975
5	0.0321	0.0064	0.0000	0.1411	0.0000	0.0492	-0.0021	0.0000	0.0000	0.0663	0.0000	0.0235
6	-0.0073	0.0044	0.0000	0.0247	0.0000	0.0087	-0.0029	-0.0015	0.0000	0.0349	0.0000	0.0145
7	0.0099	-0.0040	0.0000	0.0129	0.0000	0.0059	0.0000	-0.0030	0.0000	0.0119	0.0000	0.0049
8	0.0000	-0.0020	0.0026	0.0047	0.0000	0.0020	0.0000	-0.0013	0.0000	0.0074	0.0000	0.0027
9	0.0000	-0.0078	0.0000	0.0037	0.0000	0.0014	0.0000	0.0000	0.0000	0.0023	0.0000	0.0009
10	0.0000	-0.0022	0.0000	0.0025	0.0000	0.0012	0.0000	-0.0006	0.0000	0.0031	0.0000	0.0016
11	0.0000	-0.0025	0.0000	0.0008	0.0000	0.0002	0.0000	0.0002	0.0000	0.0004	0.0000	0.0002

Table 4.20: Multipole errors of the MQWA magnet (left aperture (l) and right aperture (r) are given).

	Normal multipoles				Skew multipoles			
n	Mean		Random		Mean		Random	
	l	r	l	r	l	r	l	r
1	-227.8	-56.4	315.9	144.2	-115.2	-57.4	225.1	148.0
2	0.0	0.0	0.0	0.0	0.0	0.0	0.0	0.0
3	0.6	-0.1	6.3	1.8	-5.6	-3.5	3.6	7.6
4	1.3	1.7	0.7	0.8	0.4	0.0	0.4	0.8
5	3.0	-2.5	1.0	0.6	2.1	1.8	1.0	1.6
6	-0.2	-0.1	0.8	0.7	0.1	0.2	0.2	0.2
7	-0.3	1.2	0.3	0.5	-0.3	-0.5	0.1	0.1
8	0.0	0.0	0.1	0.2	0.3	0.3	0.1	0.2
9	0.0	0.0	0.0	0.0	0.0	0.0	0.0	0.0
10	0.8	0.8	0.1	0.1	0.1	0.0	0.0	0.1
11	0.1	0.1	0.0	0.1	0.1	0.0	0.1	0.1
12	0.0	0.0	0.0	0.0	0.2	0.0	0.1	0.0
13	0.1	0.1	0.1	0.0	0.0	-0.1	0.1	0.1
14	-0.2	-0.2	0.1	0.1	0.1	0.1	0.0	0.1
15	0.0	0.0	0.1	0.1	0.0	0.0	0.0	0.1

Table 4.21: Multipole errors of the MQWB magnet (left aperture (l) and right aperture (r) are given).

	Normal multipoles				Skew multipoles			
n	Mean		Random		Mean		Random	
	l	r	l	r	l	r	l	r
1	-413.90	243.70	242.60	215.10	-79.30	-128.90	256.00	185.30
2	0.00	0.00	0.00	0.00	0.00	0.00	0.00	0.00
3	-45.40	50.90	11.90	4.20	-5.20	-3.60	4.40	10.90
4	1.60	1.90	1.20	1.00	0.20	0.20	0.10	0.60
5	-0.20	1.20	0.90	0.70	2.10	1.80	0.90	2.00
6	-0.30	-0.30	0.60	0.70	0.20	0.20	0.10	0.20
7	0.90	-0.40	0.40	0.40	-0.40	-0.50	0.10	0.20
8	0.10	0.10	0.00	0.10	0.30	0.40	0.30	0.20
9	0.00	0.00	0.00	0.00	0.00	0.00	0.00	0.00
10	0.90	0.90	0.10	0.00	0.00	0.10	0.30	0.00
11	0.00	0.20	0.10	0.10	0.10	0.00	0.20	0.10
12	-0.10	-0.10	0.00	0.10	0.10	0.10	0.10	0.00
13	0.20	-0.10	0.00	0.10	0.00	0.00	0.10	0.10
14	-0.20	-0.20	0.10	0.10	0.10	0.00	0.10	0.00
15	0.10	0.00	0.10	0.00	0.00	0.00	0.00	0.00

The influence of the MQM, MQML, and MQMC elements, as well as the wide aperture quadrupoles MQY was tested in view of defining target errors complying with the requirements of the dynamic aperture. In order to distinguish between the contribution of the different elements, a tracking campaign was launched where the various types of elements are included one after the other. Two variants of the optics of IR8 have been considered, the difference being the maximum horizontal beta function. The results are summarised in Tab. 4.23 and show that tighter specifications have to be defined more for the target errors of the MQM and MQY elements than the MQs. In all cases we assumed the same error distributions for all the quadrupole types. The loss of dynamic aperture is due to the large value of the beta-functions at the locations of the MQM quadrupoles (IR8) and MQY (IR4 and IR6). The main results can be summarized as follows:

- The field errors of the cold D1 / D2 are in the shadow of the main dipole and quadrupole field errors at injection.

- Using an injection optics with $\beta_{\max} \approx 500$ m in one single MQM quadrupole in IR8 and assuming the same field errors for the MQM magnets as for the arc MQ magnets shows a significant reduction of the minimum DA at injection indicating that the field quality of the insertion MQM quadrupole magnets must be better than that of the arc quadrupole magnets. Using an optics with $\beta_{\max} \leq 400$ m the reduction of the minimum DA is not significant (e.g. within the resolution of the dynamic aperture tracking studies).

- Assuming the same field errors in the wide aperture MQY insertion quadrupole magnets as for the main arc (MQ) quadrupole magnets yields a significant reduction in the minimum DA at injection. This result indicates that the field quality of the insertion MQY quadrupole magnets must be better than that of the arc quadrupole magnets. At top energy the field quality specification should be comparable to the field quality specification of the low-β triplet quadrupole magnets (comparable β-function values).

4.6 SPECIAL OPTICS SOLUTIONS

4.6.1 Alignment Optics

The determination of the triplet misalignment by means of the beam, using an optics with the triplet turned off, can be used as a complementary method for its alignment. This technique was investigated for LEP in 1993 [47] and 1995 [48] (summary in [49]). It was not used in practice for LEP because the vertical misalignment of the low-β quadrupoles could be followed easily with a sufficient accuracy by hydraulic means. The case of LEP was quite simple as there were only two vertically focusing quadrupoles contributing to the machine performance (the horizontal misalignment by the survey was sufficient). For LHC the problem is more complicated as both planes have an equal importance. However this does not mean that both LHC planes should be realigned with the same accuracy as the LEP vertical plane. A bad closed orbit correction in physics results essentially in a parasitic dispersion and a β-beating. It is sufficient that they do not increase the beam size at the interaction point and do not make synchro-betatron resonances due to a non-zero dispersion at the IP.

The LHC triplets are the main contributor to the closed orbit distortion. They must be sufficiently well aligned not to overload their correctors. The triplet corrector strength is 1.5 Tm, while the nominal integrated gradient of a single Q2 is 1306 T. The corrector can just compensate a displacement of 1.1 mm of a single Q2. This shows the importance of the relative alignment of the triplet quadrupoles.

By means of the K-modulation it is possible to determine the misalignment of the average axis of a quadrupole with respect to the neighbouring BPM's within 0.05 mm [50]. Therefore the relative misalignment of the triplet quadrupole can be checked by means of the alignment optics provided the beam reference can be well established.

If the triplets are turned off, the value of the β-functions cannot be reduced below 550m because of the large drift space between the Q4 quadrupoles. This is a situation similar to that of IR6 [25]. As the maximum possible value of the β-functions in the insertion quadrupoles is 300 m due to an aperture limit with the nominal beam, this optics can only be used with a normalized beam emittance 2.0 10^{-6}m. Such an emittance can be achieved easily by merely scraping the beam in the injectors [51].

This large value of the β-functions has another consequence that the phase advance in the region around the IR is much smaller than in the nominal optics. It is possible to partially recover this phase change, so that the tunes can be set one unit below the nominal values (Qx=63.28, Qy=58.31) if this alignment optics is set both in IR1 and IR5. The optics functions are shown on the left-hand side of Fig. 4.30. The dispersion function is not set to zero at the interaction point as the tunes have been adjusted with QF and QD. This is unimportant as long as the maximum value of the β-functions in the insertion is not increased significantly. It is also possible to turn off Q5 and Q6 on both sides of the insertion. In this case, the value of the β-functions cannot be reduced below 800 m. This optics solution is shown on the right-hand side of Fig. 4.30. According to the requirement at injection, the emittance has to be reduced to 1.4 10^{-6}m. This is a little more than the commissioning emittance, it can be achieved easily as said above.

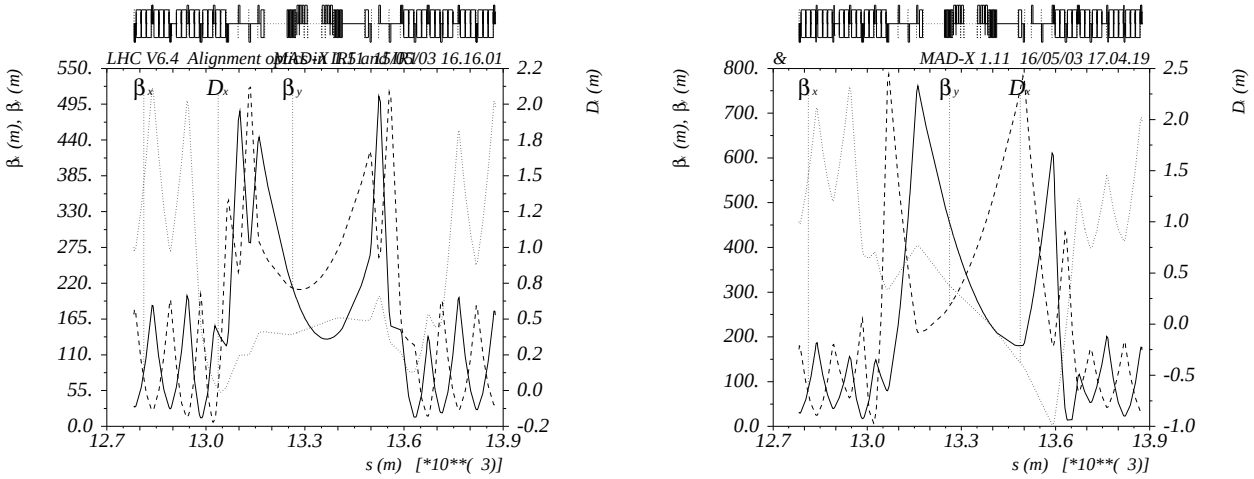

Figure 4.30: LHC alignment optics with the triplet turned off. Left: with powering of all other insertion quadrupole magnets. Right: without powering of Q5 and Q6.

For this optics the phases cannot be restored as there are not enough parameters to do it. The tunes Qx=63.72 (symmetric of the nominal tune with respect to the integer) and Qy=58.28 are obtained by changing the gradients in the main quadrupoles at the expense of introducing a β-beating of the order of one percent.

4.6.2 Resonance Free Lattices

The case where the systematic multipole components are larger than $\sim$3 limits the machine performance. This might be either because the field errors are larger than expected or because there are no correction circuits planned for the multipole type at hand. A resonance-free lattice can be used to increase the dynamic aperture. The idea behind such an optics is to adjust the phase advances per cell so that the driving terms of most non-linear resonances cancel in each arc [52]. For the LHC there are two possibilities:

- The horizontal phase advance per cell is $\frac{7}{25} \cdot 2\pi$ and the vertical one is $\frac{6}{25} \cdot 2\pi$. The associated total tunes including the insertions are Qx=68.28, Qy=59.31. The resonance free optics does not satisfy the aperture requirements in the arcs (see Sec. 4.3) and it has not been chosen as the base line optics. However, it could be run with a beam emittance reduced by 2 % and therefore presents an attractive backup solution in case the machine operation indicates performance limitations due to the systematic field errors.

  This lattice is free from resonances up to order 8 with the exception of the skew resonance 3Qy+Qx. In particular it has the nice feature of cancelling the second order chromaticity due to the systematic a_3 component.

- The horizontal phase advance per cell is $\frac{6}{25} \cdot 2\pi$ and the vertical one is $\frac{5}{25} \cdot 2\pi$. The associated total tunes including the insertions (with different insertion solution as for the previous case) are Qx=59.28, Qy=51.31. This lattice is free from resonances up to order 5. It also has the nice feature of cancelling the second order chromaticity due to the systematic a_3 component but is not limited by the mechanical aperture.

The fractional part of the tune can be adjusted by means of the phase advances over IR4 and IR6 for both cases. It has been shown that about two σ's of dynamic aperture can be gained for the case where the systematic octupole component is multiplied by a factor of three [53].

The benefits of the resonance-free lattice are preserved as long as the relative random gradient errors in the dipoles are smaller than 2×10^{-4} (three times the nominal value) [54].

4.6.3 Large β^* optics solution

The measurement of elastic scattering needs a high-β insertion so that the scattered protons have a trajectory far enough from the beam [55]. Several high-β insertions have already been studied for LHC [56, 57]. The proposal made before 2003, based on the constraint that the elastic scattering measurement was done close to D2 in the vertical plane and close to Q6 in the horizontal plane, features a quasi doublet optics [57]. It has the drawback of needing special power supplies for the Q1 quadrupole in each triplet (the connections remain standard), as well as a high current switch.

The present optics generates $\beta^* = 1540$ m without the need for a special trim power converter. The optics is shown in Fig 4.31. The vertical phase advance at the detector placed close to Q6 (220 m from the IP) is $\pi/2$ and the horizontal phase advance is $\pi/2.1$. It has been checked that this is quite acceptable for the elastic scattering measurement.

The required luminosity is low, of the order of $2 \times 10^{29}\text{cm}^{-2}\text{s}^{-1}$, as the event cross section is large. Using 156 bunches per ring, the bunches are injected in batches of four. (Alternatively the TOTEM operation can use 43 bunches where the bunches are injected one by one resulting in a lower total luminosity of approximately $10^{28}\text{cm}^{-2}\text{s}^{-1}$.

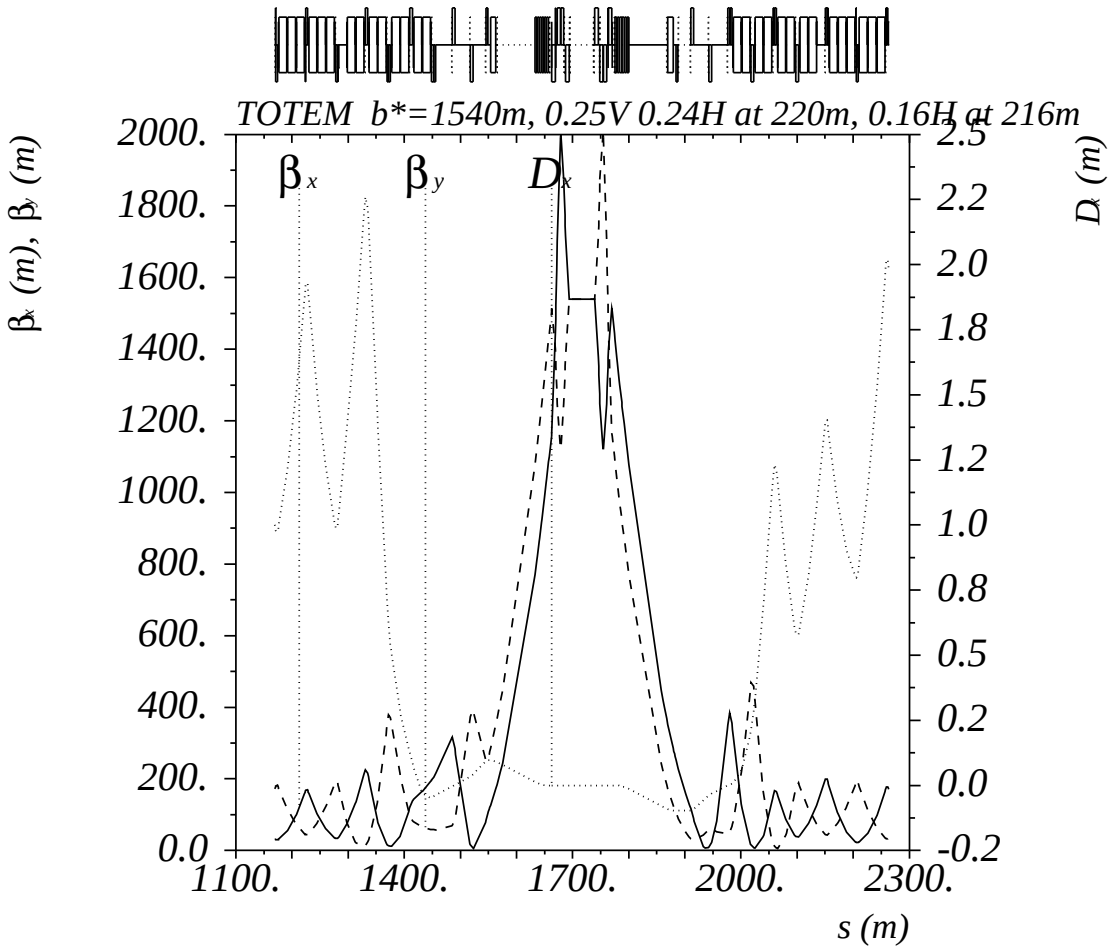

Figure 4.31: The TOTEM optics in IR5.

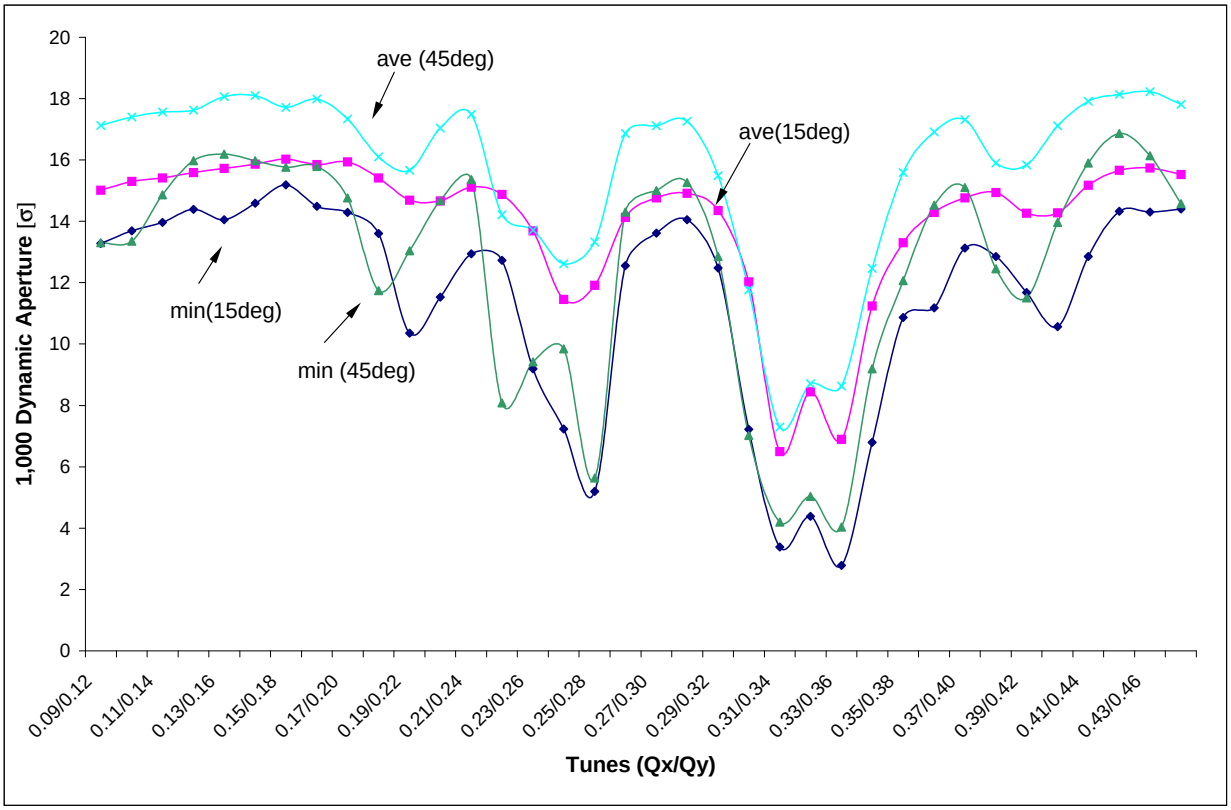

Figure 4.32: The 1000 turn DA as a function of the fractional tune for fixed distance to the (1:-1) coupling resonance.

4.7 DYNAMIC APERTURE

4.7.1 Tracking the LHC lattice

The dynamic aperture (DA) of the LHC is evaluated with the help of the SixTrack [59] simulation program. The input files for the fast tracking are generated via MAD-X [40] which is also used for the developement of the LHC optics. The dynamic aperture is defined as the maximum radius for which the particles are stable. The dynamic aperture depends on the number of turns that the simulations have been carried out for. For each phase space angle the minimum dynamic aperture is taken from 60 different sets of error distributions called seeds, in the following. This number of seeds allows the lower bound of the DA to be found with a 95% probability [60]. The phase space angle is defined as $\phi = \arctan(\sqrt{J_y/J_x})$, with ϕ =15°, 30°, 45°, 60° and 75°, where J_y and J_x are the vertical and horizontal single particle action variables [61] respectively.

The chaotic behavior of lost particles makes it impossible to predict their survival time. A typical survival plot is shown in Fig. 4.34. This also implies that the tracking mesh has to be sufficiently small to find the minimum value of the DA. For the LHC, the studies are typically performed over ranges of 2σ, each being subdivided into 30 amplitude steps. Fig. 4.32 shows the 1000 turn DA for the LHC injection optics as a function of the fractional tunes for a fixed separation between the horizontal and vertical tunes [32]. The results of such short term simulation studies have been used for optimizing the fractional part of the baseline tunes and evaluating the operational margins for the tune control at injection (see Sec. 4.4). All dynamic aperture values quoted for the LHC in the remaining part of this section are evaluated for 10^5 turns. Such intensive simulation studies have only been possible with the help of dedicated computing support [62].

Table 4.22: *Relation between target and D.A. calculated for* $x_i/y_i = 1$.

Source or Uncertainty	Impact	D.A. in σ
Target for tracking 10^5 turns		12
Finite mesh size	-5%	
Linear Imperfections[a]	-5%	
Amplitude ratio x_i/y_i plane	-5%	
Extrapolation to 4 10^7 turns	-7%	9.4
Time dependent multipoles	-10%	
Ripple	-10%	7.5
safety margin	-20%	6.0

[a] The DA reduction of 5% assumes an RMS orbit error of 0.5 mm. For an RMS orbit error of 1 mm the DA reduction can reach up to 10%.

4.7.2 Dynamic Aperture Safety Factor

Although there is a large arsenal of theoretical tools and fast tracking techniques and computers available [62], it remains impossible to track all relevant effects for sufficiently long times. Even with present day computers it is not possible to perform a full scale simulation over 4×10^7 turns, which corresponds to 1h of beam storage time. The DA obtained from simulations is typically 20% too optimistic when compared with dedicated beam experiments at several accelerators. Therefore, to ensure that particle motion is sufficiently linear at an amplitude relevant for the collimation system, i.e. roughly 6 σ, we estimate that the simulated DA should be a factor 2 larger. That this factor is valid in the absence of the very strong beam beam interaction which should be treated separately.

Typical simulation runs for the LHC DA are for 10^5 turns with non-linear field errors only, with empirical tune and chromaticity correction, and a 'perfect' powering of the non-linear lattice spool piece circuits based on the error distribution in the main dipole magnets. Tab 4.22 explains the different contributions which enter into this 'extrapolation' factor [63]. The DA reduction due to the linear imperfections and due to an imperfect spool piece circuit powering, have been studied in Ref. [35] and [36]. Assuming a perfect b_4 spool piece powering the linear field errors (quadrupole misalignment and closed orbit correction to 1 mm rms plus b_2 errors to generate a β-beat between 25 % and 35 %) reduce the minimum DA from 11.7 σ to 11.3 σ. Without b_4 correction via the b_4 spool piece circuits the same errors reduce the minimum DA from 11.2 σ to 9.6 σ. The DA reduction due to errors in the spool piece circuit powering is shown in Fig. 4.33. Depending on the spool piece circuit and the mispowering error scenarios the minimum DA can drop by, is up to 30 %.

Taking a conservative approach these contributions are added linearly. The 'finite mesh size', 'amplitude ratio' and the 'extrapolation' reflect the limited computing capacity which limits the speed of the computation and how fine a simulation mesh can be chosen. It is known from existing hadron storage rings that there are effects that limit the performance of any new machine. It is very hard to predict by how much the LHC will suffer from lattice imperfections, power supply ripple and transient effects. Finally a 20% margin is taken as a measure of the lack of predictability of tracking simulations. In the absence of beam-beam interaction the target DA for the simulations should therefore be about 12 σ.

4.7.3 Dynamic Aperture at Injection and Collision

Tab 4.23 and 4.24 summarize the dynamic aperture results for the LHC studies at injection and collision energy with luminosity optics respectively. Fig. 4.35 shows the case of non-linear main dipole, main quadrupole and warm quadrupole field errors as an example of the tracking results as a function of the angle of initial amplitudes. All tracking studies presented in this Chapter have been done with nonlinear field errors up to a_{11} and b_{11} and include tune and chromaticity (target $Q^{'} = 2$), linear and chromatic coupling, b_3, b_4 and b_5 corrections. While tracking simulations provide the most accurate evaluation of the DA the tracking results as such are not well suited for guiding the evolution of the field quality specification in case of an insufficient DA [64]. The LHC tracking studies have therefore been complemented by studies on DA limitations due to single selected multipole components [65][66] and their first-order resonances (or sub-resonances) [7] and [8]

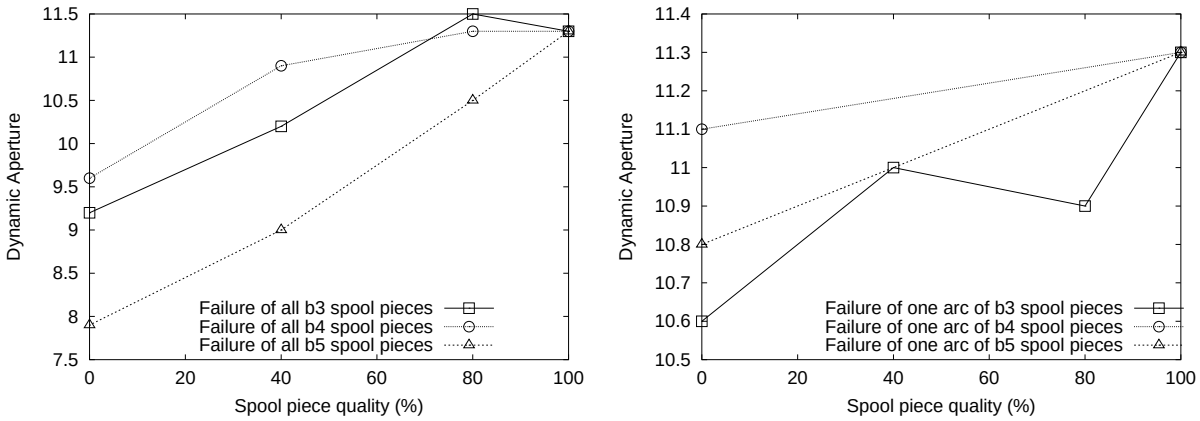

Figure 4.33: The minimum dynamic aperture (in units of the RMS beam size) as a function of b_3, b_4 and b_5 spool piece quality at injection. 100 % represents full correction and 0 % none. The chromaticity ($Q^{'}$) and the tunes are corrected to their nominal values in all cases using the lattice sextupole and tuning quadrupole circuits. Left: mispowering of all spool piece circuits. Right: mispowering of the spool piece circuits in the arc between IR2 and IR3.

and by frequency map, resonance strength and diffusion speed analysis [67]-[69] and other 'indicators' for the DA [70][71]. A summary of the different methods for calculating the DA can be found in [72] and a selection of references for the DA tracking studies at injection energy can be found in [73].

All results shown in Tab. 4.23 just satisfy the goal of a $12\ \sigma$ DA for 10^5 turn tracking within the resolution of the numerical simulations ($\pm 0.5\ \sigma$) indicating that the specified field errors are at their acceptible limits. The fact that the last case in Tab 4.23 for the cross section 2 is only 11.2 σ is related to the fact that the systematic b_5 and b_7 field errors are outside the specification of 1.4 and 0.33 units instead of 1.1 and 0.1 units respectively. All other multipoles, random and systematic, meet the specifications given in [33].

The nominal correction scheme of the low-beta triplet errors has been investigated for the LHC V6.2 in collision but without beam-beam interactions. Fig. 4.36 shows the average and minimum dynamic apertures among the 60 seeds for 10^5 turn tracking. The triplet errors reduce the average and minimum dynamic aperture to $12.9\ \sigma$ and $8.8\ \sigma$ respectively. This is mainly due to the large b_6 component of the triplet errors. After applying the local triplet corrections of b_3, b_4, b_6, a_3 and a_4 as described in Ref. [74], the average and minimum dynamic aperture increase to $16.8\ \sigma$ and $12.9\ \sigma$ respectively, i.e. larger by some $4\ \sigma$. We can therefore conclude that the triplet correction scheme is indeed effective for LHC lattice version V6.2.

In collision the DA is dominated by the beam-beam interactions and the goal for the field error specification is to keep the DA due to the magnet field errors in the shadow of the beam-beam interactions. The target DA for the 10^5 turn tracking for collision configuration is 10 σ. In collision the triplet errors are considered with and without their corrections and the D1/D2 field errors are treated without correction by the triplet corrector system. A comparison of these cases shows that the cold D1/D2 field error are in the shadow of the triplet field errors and that the triplet field errors are only relevant for $\beta^* \leq 0.75$ m [75]. For $\beta^* \geq 0.75$ m the DA is above 10 σ even without triplet field error correction. Studies including the beam–beam interactions are discussed in detail in Chap. 5.

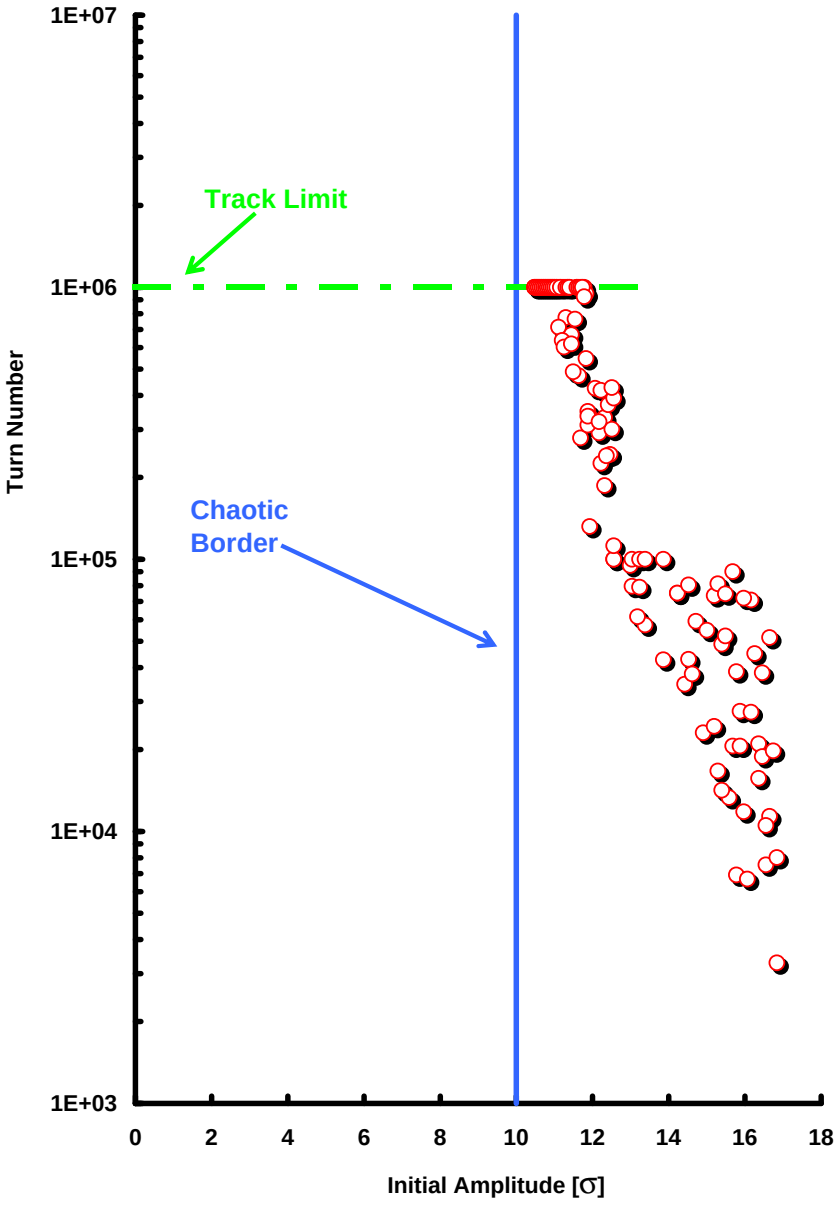

Figure 4.34: Typical Survival Plot

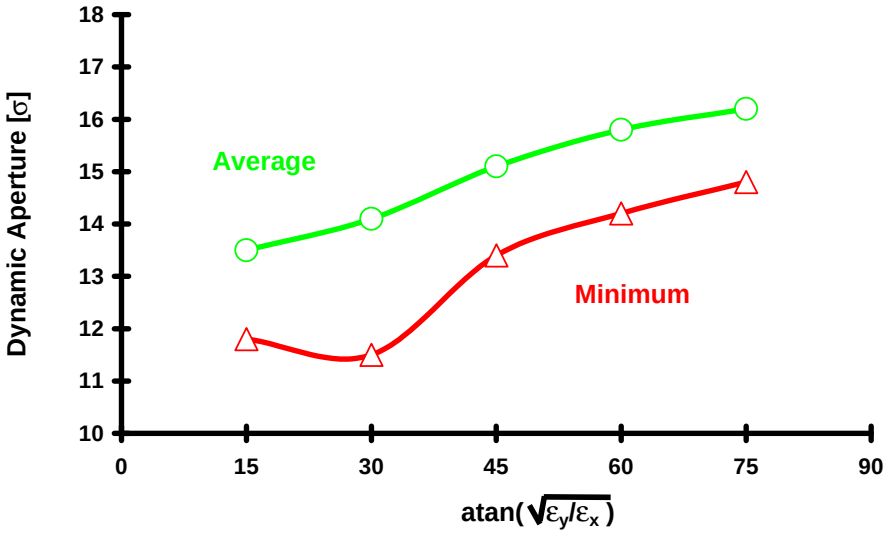

Figure 4.35: Average and minimum dynamic apertures of LHC V6.4 including realistic errors of the warm Quadrupoles MQW, the tracking has been performed for 10^5 turns.

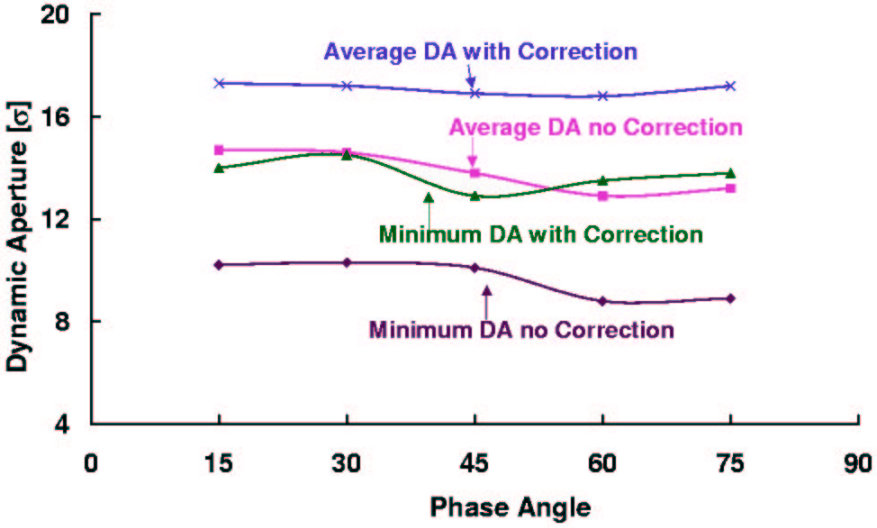

Figure 4.36: Average and minimum dynamic apertures with and without the correction of low–beta triplet field errors. The beam–beam interaction is not included and the tracking has been performed for 10^5 turns.

Table 4.23: Average and minimum 10^5 turns dynamic aperture at injection energy for 5 phase space angles $\phi = \arctan(\sqrt{J_y/J_x})$ of the phase space. All simulations were done for 60 seeds with lattice corrector circuit powering and refer to LHC injection optics Version 6.2 or 6.4 with nominal tunes $Q_x = 64.28$ and $Q_y = 59.31$.

Dyn. Aper. $[\sigma]$	15°	30°	45°	60°	75°
LHC V6.2, Error table 9901 [76] with errors in the MB and MQ elements					
Minimum	11.8	11.8	13.4	13.9	15.0
Average	13.3	13.6	15.3	15.5	16.1
LHC V6.2, Specification table [33] with errors in the MB and MQ elements					
Minimum	11.5	11.6	12.4	12.9	14.5
Average	12.7	13.1	≥ 13.9	≥ 14.0	≥ 14.6
Minimum	9.3	10.1	11.4	11.1	11.7
Average	11.3	12.0	12.7	12.9	12.7
LHC V6.4, Field error expected after the production of 60 collared coils (X-section 2) with errors in the MB and MQ elements [77], [78]					
Minimum	**11.2**	12.0	13.3	15.2	14.8
Average	12.2	13.4	14.7	16.8	15.9
LHC V6.4, Error table 9901 [76] with errors in the MB and MQ elements plus field errors in warm quadrupole magnets [44]					
Minimum	11.7	11.2	13.0	13.8	14.3
Average	13.5	14.0	≥ 15.0	≥ 15.6	≥ 16.0
LHC V6.4, Specification table [33] with errors in the MB and MQ elements plus field errors in the cold D1 and D2 dipole magnets [41]					
Minimum	11.3	12.2	13.9	16.3	15.5
Average	12.2	13.7	14.8	17.3	16.3
LHC V6.4, Specification table [33] with errors in the MB and MQ elements plus field errors in the cold D1 and D2 dipole and the MQM insertion quadrupole magnets using an IR8 optics with $\beta_{\max} = 500$ m at one MQM location (Q6) [41]					
Minimum	10.3	11.5	13.4	14.7	14.0
Average	12.0	13.2	14.5	16.3	15.2
LHC V6.4, Specification table [33] with errors in the MB and MQ elements plus field errors in the cold D1 and D2 dipole and the MQM insertion quadrupole magnets using an IR8 optics with $\beta_{\max} \leq 400$ m at one MQM location (Q6) [41]					
Minimum	10.8	11.9	13.5	14.9	14.1
Average	12.2	13.3	14.6	15.9	15.0
LHC V6.4, Specification table [33] with errors in the MB and MQ elements plus field errors in the cold D1 and D2 dipole and the MQM and MQY insertion quadrupole magnets [41]					
Minimum	9.27	10.1	11.4	11.1	11.7
Average	11.3	12.0	12.7	12.9	12.7

Table 4.24: Average and minimum 10^5 turns dynamic aperture at collision energy for 5 phase space angles $\phi = \arctan(\sqrt{J_y/J_x})$ of the phase space. All simulations are done for 60 seeds with different field error sources and correction schemes and refer to LHC collision optics Version 6.2 or 6.4 with nominal tunes Q_x =64.31 and Q_y =59.32.

Dyn. Aper. $[\sigma]$	15°	30°	45°	60°	75°
LHC V6.2, $\beta^* = 0.5$ in IR1 and IR5 with triplet field errors and NO correction [74]					
Minimum	10.2	10.3	10.1	8.8	8.9
Average	14.7	14.6	13.8	12.9	13.2
LHC V6.2, $\beta^* = 0.5$ in IR1 and IR5 with triplet field errors and correction [74]					
Minimum	14.0	14.5	12.9	13.5	13.8
Average	17.3	17.2	16.9	16.8	17.2
LHC V6.4, $\beta^* = 0.5$ in IR1 and IR5 and $\beta^* = 1.0$ in IR8 with triplet, MB, MQ and cold D1 and D2 field errors and b_3, b_4 and b_6 triplet field error correction (no correction for a_3 and a_4[44])					
Minimum	12.3	11.7	10.8	10.8	11.0
Average	14.7	14.4	14.1	14.0	14.1
LHC V6.4, $\beta^* = 0.5$ in IR1 and IR5 and $\beta^* = 1.0$ in IR2 with triplet and cold D1 and D2 field errors [44] and triplet field error correction					
Minimum	11.5	11.5	10.8	10.3	11.3
Average	15.4	15.0	14.1	14.4	15.1
LHC V6.2, $\beta^* = 0.5$ in IR1 and IR5 with triplet field errors and beam-beam interactions: NO triplet correction [74]					
Minimum	**6.6**	6.1	7.0	7.5	7.9
Average	8.4	8.4	8.7	8.6	9.2

REFERENCES

[1] Baseline chage request 53 approved by the U.S. LHC collaboration by summer 2003. An Engeneering Change Request is currently (August 2003) under preparation at CERN.

[2] A. Faus-Golfe et al, 'A more robust and flexible lattice for LHC', Proceedings of the 1998 European Particle Accelerator Conference, Stockholm Sweden, June 1998

[3] W. Scandale, 'Revisiting the Problem of the LHC Insertion Symmetry', CERN SL/Note 94-42 (AP), April 1994

[4] A. Faus-Golfe et al, 'Modular opticsal design of the LHC experimental insertions', Proceedings of the 1996 European Particle Accelerator Conference, Sitges Spain, June 1996

[5] J.P. Koutchouk, Alternative magnetic Optics for LEP1, CERN SL/91-23(DI), Chamonix 1991

[6] J.P. Koutchouk, 'Decoupling of a strongly coupled lattice with an application to the LHC', LHC Project Report 15, July 1996

[7] R. Talman, 'Tune optimization for maximum dynamic acceptance, 1, formulation', LHC Project Report 197, July 1998

[8] R. Talman, 'Tune optimization for maximum dynamic acceptance, 2: Qx=65, Qy=58', LHC Project Report 233, August 1998

[9] A. Verdier, 'Resonance free lattices for A.G. machines', Proceedings of the 1999 Particle Accelerator Conference, New-York, U.S.A, 1999

[10] D. Kaltchev, F. Schmidt and A. Verdier, 'Robustness of Resonance free lattices against gradient errors', LHC Project report 475, August, 2001

[11] O. Brüning, W. Herr and R. Ostojic; *A beam separation and collision scheme for IP1 and IP5 at the LHC for optics version 6.0*, LHC Project Report 315 CERN, (1999).

[12] O. Brüning, W. Herr and R. Ostojic; *A beam separation and collision scheme for IP2 and IP8 at the LHC for optics version 6.0*, LHC Project Report 367 CERN, (1999).

[13] V. Baglin, I. Collins and N. Kos, Beam Screens for the LHC Long Straight Sections, Functional Specification EDMS doc. 334961, LHC-VSS-ES-0002 rev 1.0, Geneva, CERN (April 2003).

[14] O.S. Brüning, Optics Solutions in IR1 and IR5 for Ring-1 and Ring-2 of the LHC Version 6.0, CERN-LHC-Project-Note-187, Geneva, CERN (April 1999).

[15] O. Brüning; *Optics solutions in IR2 for Ring 1 and Ring 2 of the LHC Version 6.0*, LHC Project Note 188 CERN, (1998).

[16] 'LHC Version 6.4: Layout of the DFBAs in the Insertion Regions', ECR LHC-LS64-EC-0002

[17] J.B. Jeanneret, CERN LHC Project Note 115,1997.

[18] T. Trenkler and J.B. Jeanneret, The principles of two-stage betatron and momentum collimation in circular accelerators, Part.Acc., **50** , (1995) 287, January 1995.

[19] J.B. Jeanneret, Phys.Rev. ST-AB, **1**, 081001, Dec. 1998.

[20] D.I. Kaltchev et al., CERN LHC Project Report 134 and PAC1997,1997.

[21] D.I. Kaltchev et al., CERN LHC PRoject Report 305 and PAC1999,1999.

[22] D.I. Kaltchev et al., CERN LHC PRoject Report 194 and EPAC98,1998. CERN,1997.

[23] A. Verdier, A tunable insertion for point 4 in LHC. LHC Project Note 93 (June 1997).

[24] A. Verdier, Phases between IP's and non-linear chromaticity. LHC Project Note 103 (August 1997).

[25] A. Verdier, The LHC IR6 optics. LHC Project Note 146 (June 29, 1998).

[26] J.-B.Jeanneret and T.Trenkler, The principles of two stage betatron and momentum collimation in circular accelerators, LHC Note 312

[27] T. Risselada, Optical Requirements for an LHC Cleaning Insertion with Elliptical Collimators, SL/Note 95-67 (AP)

[28] O. Brüning; *Optics solutions in IR8 for Ring 1 and Ring 2 of the LHC Version 6.0*, LHC Project Note 188 CERN, (1998).

[29] J.B. Jeanneret and R. Ostojic, CERN LHC PRoject Note 111,1997.

[30] J.B Jeanneret at the 43rd PLC, October 1998 and decisions therein.

[31] V. Bagin, I. Collins and N. Kos, LHC-VSS-ES-0002 rev 1.0, EDMS doc 334961.

[32] L. Jin and F. Schmidt, 'Dynamic aperture tune scan for LHC version 5 at injection energy', LHC Project Note 182, January 1999

[33] S. Fartoukh, O. Brüning, Field quality specification for the LHC Main dipole Magnets, LHC-Project-Report-501, Geneva, CERN (October 2001).

[34] Proceedings of the 'Workshop on Collective Effects in Large Hadron Colliders', Particle Accelerators, Volume 50, Numbers 1-3, 1995.

[35] M. Hayes, "The effect of spool piece mispowering on the dynamic aperture of the LHC during injection', LHC Project Report 522, December 2001

[36] M. Hayes, 'Tolerances of the spool piece correction system for the LHC', LHC Project Report 590, July 2002

[37] R. Wolf, Field Error Naming Conventions for LHC magnets, Engineering Specification LHC-M-ES-0001, Geneva, CERN (October 2001).

[38] A. Verdier (ed.) et al, Report on the mini-workshop on the LHC alignment, LHC-Project-Note-247, Geneva, CERN (February 2001).

[39] J.P. Koutchouk and A. Verdier, 'Specification for the field quality of the LHC closed orbit correctors and sextupoles', LHC Project Note 210, January 2000.

[40] H. Grote and F. Schmidt, MADX an upgrade for MAD8. PAC03 Portland, Oregon, May 2003.

[41] S. Fartoukh, M. Giovannozzi, A. Verdier, Tolerances for the quadrupoles of the Special Straight Sections, in preparation.

[42] M. Giovannozzi, presentation at the 3rd LTC Meeting, http://lhcp.web.cern.ch/lhcp/ab-ltc/ltc_2003-03.html (2003).

[43] M. Giovannozzi, T. Risselada, F. Schmidt, 'Effect of the field quality of warm quadrupoles in IR3 and IR7 on LHC performance', in preparation.

[44] O. Brüning, S. Fartoukh, M. Giovannozzi, T. Risselada, 'Dynamic Aperture Studies for the LHC Separation Dipoles', in preparation.

[45] E. Boter, G. de Rijk, Multipole tables for the MQWA and MQWB magnets, LHC Project Note 289 (2002).

[46] E. Willen, Superconducting beam separation dipoles, LHC-MBR-ES-0001 rev. 2.0, (2000).

[47] F. Bordry, P. Collier and A. Verdier, Check of the BPM alignment with the LEP beam. SL MD Note 99 (September 6, 1993).

[48] A. Verdier, Estimation of the vertical misalignment of the low-β quadrupoles in IP2 and IP6. SL-MD Note 188 (October 24, 1995).

[49] A. Verdier and S. Weisz, Alignment of low-β with beam. Proc. of the fourth International Workshop on Accelerator Alignment. KEK Proceedings 95-12 (January 1996).

[50] I. Barnett et al., Dynamic beam based calibration of orbit monitors at LEP. Proc. of the fourth Int. Workshop on accelerator alignment IWAA95, KEK, November 1995. KEK Proceedings 95-12 (January 1996).

[51] G. Arduini, A. Verdier, Poor man pilot and TOTEM bunches. AB-Note-2003-017 MD (February 12, 2003).

[52] A. Verdier, Resonance-free lattices for A.G. machines. PAC 1999 New-York. Also divisional report CERN-SL-99-018 AP.

[53] F. Schmidt and A. Verdier, Optimisation of the LHC dynamic aperture via the phase advance of the arc cells. PAC 1999 New-York. Also LHC project report 297.

[54] F. Schmidt, A. Verdier, D. Kaltchev, Robustness of resonance-free lattices against gradients errors. PAC2001 Chicago USA (June 2001). Also LHC Project Report 475 (August 2001).

[55] The TOTEM collaboration, Technical proposal. CERN/LHCC 99-7, LHCC/ P5 (15 March 1999).

[56] A. Faus-Golfe, J. Velasco and M. Haguenauer, Precise measurements of the total cross section and the coulomb scattering at the LHC. EPAC 2000 (Vienna).

[57] A. Faus-Golfe, A. Verdier, Optics studies for diffractive physics at the LHC. EPAC 2002 (Paris).

[58] S. Weisz, An analytic approach to a high-β insertion and possible application for TOTEM at the LHC. LHC project note 164 (September 1998).

[59] F. Schmidt, "SixTrack, version 3, single particle tracking code treating transverse motion with synchrotron oscillations in a symplectic manner", CERN SL/94–56 (AP) (1994) F. Schmidt, "Run Environment for SixTrack", Beam Physics Note 53,

[60] H. Grote, "Statistical significance of dynamic aperture calculations", Beam Physics Note 34.

[61] L. Jin and F. Schmidt, "Tune Scan Studies for the LHC at Injection Energy", LHC Project Report 377.

[62] E. McIntosh, T. Pettersson and F. Schmidt, A Proposal for a Numerical Accelerator Project, Part. Acc. Vol. 54 (2-4) (1996).

[63] J.P. Koutchouk, 'The LHC Dynamic Aperture', Proceedings of the 1999 Particle Accelerator Conference, New York, 1999

[64] M Böge, H. Grote, Q. Quin and F. Schmidt, Dynamic Aperture Studies for the LHC Version 4, LHC Project Report 31, July 1996

[65] S. Wiesz and Q. Quin, Study of Systematic Multipolar Errors in LHC Version 4.1 and Spool Pieces Compensation, LHC Project Note 42, March 1996

[66] Y. Luo and F. Schmidt, "LHC Dynamic Aperture versus single Multipole Components", LHC Project Note 272,

[67] Y. Papahilippou, Correction Schemes for the Normal Octupole and Decapole Errors in the LHC Dipole, CERN LHC Project Report 411

[68] Y. Papaphilippou, Frequency Maps of LHC Models, CERN LHC Project Report 299

[69] Y. Papaphilippou and F. Schmidt, Normal Form Approached and Resonance Analysis of LHC Models, CERN LHC Project Report 255

[70] R. Bartolini, A. Faus-Golfe, M. Giovannozzi, E. Todesco, W. Scandale, Early Indicators of Long Term Stability in Hadron Colliders, LHC Project Report 41, July 1996

[71] M. Giovannozzi, W. Scandale, E. Todesco, Prediction of Long-Term Stability in Large Hadron Colliders, LHC Project Report 45, July 1996

[72] M. Böge et al, Overview of the LHC Dynamic Aperture Studies, CERN LHC Project Report 106 and in the Proceedings of the 1997 Particle Accelerator Conference, New York, U.S.A.

[73] F. Schmidt and A. Verdier, "Optimisation of the LHC dynamic aperture via the phase advance of the arc cells", 1999 Particle Accelerator Conference - PAC '99 New York City, NY, USA , LHC Project Report 297 L. Jin, Y. Papaphilippou and F. Schmidt, "Improvement of LHC Dynamic Aperture via Octupole Spool Pieces for the Nominal Tunes", LHC Project Report 253 M. Böge, H. Grote, Q. Qin and F. Schmidt, "Dynamic Aperture Studies for the LHC Version 4", LHC Project Report 31, paper presented at the Fifth EPAC Conference, Barcelona, June 1996 W. Fischer and F. Schmidt, "Long–term tracking for the LHC including ripple", CERN SL/Note 94–75 (AP) F. Galluccio, Z. Guo, W. Scandale, F. Schmidt and A. Verdier, "Long–term stability studies for the Large Hadron Collider", CERN SL/91–20 (DI), LHC Note 147, in Conference Record of the 1991 IEEE Particle Accelerator Conference, San Francisco, California, May 1991, pp. 1669–1671 F. Schmidt, "First tracking results with SixTrack for the LHC", CERN SPS/AMS/FS (1988)

[74] Y. Luo and F. Schmidt, "Weak–Strong Beam–Beam Tracking for LHC V6.0 ", LHC Project Report 502 Y. Luo and F. Schmidt, "Dynamic Aperture Studies for LHC Optics Version 6.2 at Collision", LHC Project Note 310 H. Grote, L.H.A. Leunissen and F. Schmidt, "LHC Dynamic Aperture at Collision", LHC Project Note 197

[75] M. Hayes, 'The effect of triplet errors, misalignments and associated correction systems on dynamic aperture', LHC Project Note 291, April 2002.

[76] S. Fartoukh, Installation scenarios and dynamic aperture LHC-Project-Report-449, Geneva, CERN (December, 2000).

[77] E. Todesco et al., An Estimate of Multipolar Errors in the LHC Dipoles, LHC-Project-Report-625, Geneva, CERN (December 2002).

[78] S. Fartoukh, Session 6 of the Workshop on Field quality Steering of the LHC Dipole, `http://lhc-div-mms.web.cern.ch/lhc-div-mms/MMSPAGES/MA/fqwrkshp/fqwrkshp.html`, Geneva, CERN (March 2003).